Design of Efficient Power Converters for Electric Vehicle Charging and Vehicle-to-Grid Applications

by

© Burak Muhammetoglu, BSc

A thesis submitted to the School of Graduate Studies
in partial fulfillment of the requirements for the
degree of Master of Engineering.

Department of Electrical and Computer Engineering

Memorial University

May 2025

St. John's, Newfoundland and Labrador, Canada

Abstract

This research presents the design and optimization of bidirectional Dual Active Bridge (DAB) converters for electric vehicle battery charging applications, encompassing both heavy and light electric vehicles. The core of the studies is a 5.6 kW DAB converter that can seamlessly transition between 3.7 kW and 11.2 kW power outputs to accommodate different vehicle requirements without the need for circuit component changes. This flexibility is achieved through the novel integration of interleaved and parallel operation capabilities, allowing for efficient operation across a broad power range.

Key innovations include the design of a high-frequency transformer with dual secondary outputs to facilitate power transfer at high currents up to 30 A, optimizing thermal design and minimizing the stress on the circuit board. The use of next-generation power semiconductors and low-loss magnetic circuit elements has resulted in an optimized single-stage bidirectional converter design that showcases enhanced efficiency and competitiveness in the field. Furthermore, the converters design enables easy reconfiguration to meet the desired power output, vehicle type, and application needs, making it adaptable for future applications such as Vehicle-to-Grid (V2G) systems.

The combination of these features, versatility in power output, efficient high-current transfer, innovative use of power semiconductors, and adaptability for future technologies—positions this DAB converter as a significant advancement in electric vehicle charging technology, offering a scalable solution to meet the evolving demands of electric mobility and renewable energy integration.

Acknowledgements

First and foremost, I would like to express my heartfelt gratitude to my supervisor, Dr. Mohsin Jamil, for his invaluable guidance, support, and encouragement throughout my research. His insightful comments and immense knowledge have been crucial in the completion of this thesis.

I am also deeply thankful to my family for their unconditional, unwavering support and sacrifices, which have been instrumental in my academic journey.

Co-authorship Statement

I, Burak Muhammetoglu (B.M.), am the primary author and copyright holder of all chapters in this thesis. The simulations, methods, figures, tables and experiments were developed by me, B.M. The manuscripts within this thesis are co-authored by my supervisor, Dr. Mohsin Jamil (M.J.), who contributed significantly to the revision and editing of the manuscripts and this thesis.

Additionally, Dr. M.J. reviewed the experimental procedures and provided valuable suggestions for improvements. In this thesis, four publications are presented, all of which have either been completed or are currently undergoing the peer-review process. I, Burak Muhammetoglu (B.M.) am the primary author for all the publications. The publications are listed under the “List of Publications” subsection.

Table of Contents

List of Tables

List of Figures

List of Abbreviations

G2V	Grid-To-Vehicle
V2G	Vehicle-To-Grid
DC	Direct Current
AC	Alternating Current
VA	Volt-Ampere
HF	High-Frequency
LV	Low-Voltage
DAB	Dual Active Bridge
IGBT	Insulated Gate Bipolar Transistor
MOSFET	Metal Oxide Semiconductor Field Effect Transistor
L	Inductor
C	Capacitor
LLC	Inductor-Inductor-Capacitor
RMS	Root Mean Square
ZCS	Zero Current Switching
ZVS	Zero Voltage Switching
CC	Constant Current
CV	Constant Voltage
PWM	Pulse Width Modulation
PCB	Printed Circuit Board
SOC	State of Charge
FEC	Front-End Converter
PLL	Phase-Locked-Loop
ESR	Equivalent Series Resistance
ESL	Equivalent Series Inductance
SiC	Silicon-carbide

List of Symbols

kW	Kilowatt
V	Voltage
A	Ampere
Ω	Impedance (Ohms)
Hz	Hertz (Frequency)
kHz	Kilohertz (Frequency)
P	Power (Watts)
F/mF	Farad/miliFarad (Capacitor Value)
H/mH	Henry/milliHenry (Inductor Value)
C_{DC2}/L_{DC2}	DC Inductance/Capacitance
vAC2	AC Voltage
n	Transformer Turn Ratio
C_{OSS}	Low Output Capacitors
D	Duty Cycle
θ	Phase Shift Value on the AC Side
SPS	Single-Phase Shift
S1,S2..S8	Switches S1-S8
XL	Reactance Value of the Energy Transfer Inductor
R_{DS}	Conduction Resistance (On-Resistance)
V_{GS}	Gate-Source Voltage (Silicon Carbide Switch)
V_{DS}	Drain-Source Voltage
I_{DS}	Drain-Source Current

1. Introduction

1.1. Problem Statement

Bidirectional DC-DC converter topologies have become an attractive option in recent years, especially for renewable energy and electric vehicle technologies. The general block diagram of elements included in galvanically isolated bidirectional DC-DC converter topologies is shown in Figure 1 alongside the EV charging elements, which are shown in black. Accordingly:

a) The filter structure located at the input and output is used to obtain a smooth DC terminal voltage and current.
b) The DC-AC converter consists of a structure made of semiconductor switch elements and is responsible for providing AC power to the high-frequency (HF) transformer. The AC-DC converter structure provides DC power to the respective input or output terminal using switches. Both converters include elements that allow for bidirectional power flow. Typically, full-bridge, half-bridge, and push-pull circuit structures are used in these configurations. Moreover, literature includes a bidirectional single-switch cross converter topology as presented in references [1], [2].

c) The leakage inductances in the HF transformer provide energy storage capability in the AC part, altering the switching current waveforms and thus enabling low switching losses. This structure is not necessary for every bidirectional DC-DC converter. Practically, these are shown as parasitic elements of the HF transformer.

d) The HF transformer is required for electrical isolation. In addition to isolation, it provides a high voltage and current transfer ratio [3]. The HF transformer is more size-efficient compared to low-frequency transformers. However, converter losses increase in high-frequency operating converters, hence the most suitable switching frequency for the topology needs to be determined.

The isolated bidirectional DC-DC converter block diagram shown in Figure 1 is referred to as a single-stage topology [4]. These topologies consist of a minimum number of converter stages. The number of required elements is lower compared to other multi-stage topologies. Nevertheless, operating across a wide input and output voltage variation range can lead to inefficient use of transformers and switch elements.

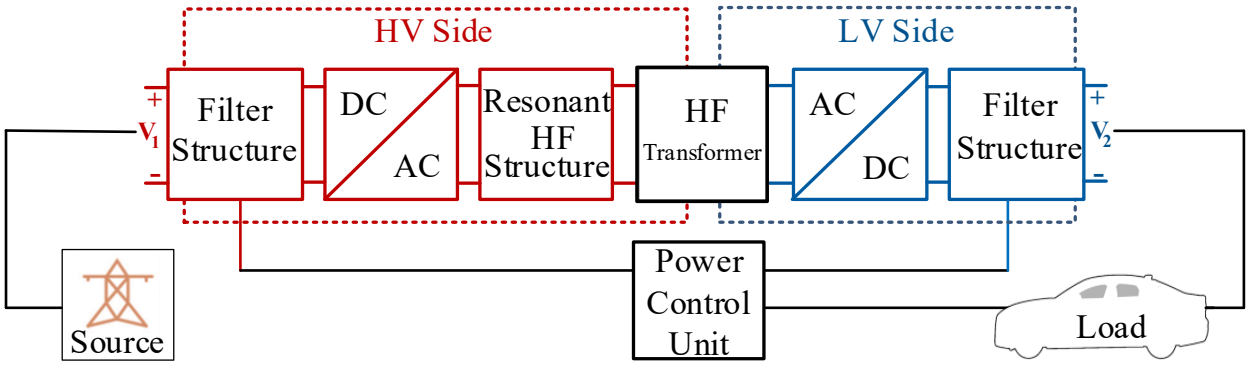

Figure 1. Block Diagram of Basic Structures in an Isolated Bidirectional DC/DC Converter

The effective use of transformers and semiconductor switches is achieved with multi-stage topologies, and these structures adjust voltage and current levels by including additional power converters [3].

1.2. Motivation and Research Objectives

1.2.1. Motivation

The electrification of transportation is rapidly gaining momentum as a critical component in the global effort to reduce carbon emissions and transition towards sustainable energy sources. Electric vehicles (EVs) offer significant potential to decrease reliance on fossil fuels, yet their widespread adoption is challenged by the need for efficient, reliable, and scalable charging infrastructure. A key element in this infrastructure is the design of power converters that can efficiently manage the bidirectional flow of electricity between the grid and the EVs, facilitating not only charging but also the integration of renewable energy sources through Vehicle-to-Grid (V2G) technology. This capability enables EVs to act as distributed energy storage systems, contributing to grid stability and supporting renewable energy integration.

However, the design of power converters that can operate efficiently across a wide range of power levels and vehicle types, while minimizing energy losses and maintaining compactness, remains a significant technical challenge [4]. Current solutions often face limitations in scalability, efficiency, and the ability to handle high currents and voltages, particularly in scenarios involving heavy-duty vehicles. To address these challenges, this research focuses on the development and optimization of a bidirectional Dual Active Bridge (DAB) converter designed for both light and heavy EV applications. The converter's unique design features, including high-frequency transformers and advanced semiconductor technologies, aim to achieve high efficiency, versatility, and scalability, positioning it as a key component in the future of EV charging infrastructure.

1.2.2. Research Objectives

The primary objectives of this research are as follows:

- Design and Optimization of a DAB Converter: Develop a bidirectional DAB converter with the ability to operate efficiently across a wide range of power outputs (3.7 kW to 11.2 kW) to accommodate both light and heavy electric vehicles. This involves optimizing the design of high-frequency transformers and the integration of advanced semiconductor technologies to enhance efficiency and reduce thermal stress.

- Dynamic Performance Analysis: Perform comprehensive simulations using MATLAB/Simulink to analyze the dynamic performance of the designed converter under various operational conditions, including different power levels and input voltages. These simulations will be used to validate the converter's efficiency and adaptability.

- Experimental Validation: Conduct hardware experiments to validate the simulation results and assess the converter's real-world performance. This includes evaluating power semiconductor losses, conduction losses, and overall thermal management to ensure reliability under operational stress.

1.3. Structure of Thesis

The structure of this thesis is meticulously organized to address the various challenges associated with the design, optimization, and validation of bidirectional DAB converters for EV charging and V2G applications. Each chapter builds upon the previous one, providing a comprehensive exploration of the technical and practical aspects of this research. The following is an in-depth overview of each chapter:

- Introduction and Literature Review:

  This chapter lays the foundation for the research by presenting the background and significance of efficient power conversion systems in the context of electric vehicle charging infrastructure. It begins with a problem statement, emphasizing the need for scalable and efficient power converters that can support the growing demand for electric mobility and renewable energy integration. The chapter includes an extensive literature review, covering bidirectional DC-DC converter types, particularly focusing on DAB topologies. The chapter also reviews the challenges associated with high-frequency transformer design, semiconductor losses, and thermal management in power converters, setting the stage for the research objectives and methodology sections.

- Design and Theoretical Analysis of the DAB Converter:

  In this chapter, the design methodology for the bidirectional DAB converter is discussed in detail. The chapter begins with a comprehensive explanation of the DAB topology, including the selection of components such as high-frequency transformers and power semiconductors. The design process is guided by the need to achieve high efficiency across a wide power range, suitable for both light and heavy electric vehicles. The chapter includes detailed calculations for component sizing, loss analysis, and thermal management strategies. Special attention is given to the integration of silicon carbide (SiC) and silicon (Si) semiconductors, analyzing their impact on converter performance. Theoretical models are developed to predict the converter's behavior under various operating conditions, providing the necessary groundwork for subsequent simulation and experimental validation.

- Simulation and Dynamic Performance Evaluation:

  This chapter analyses the dynamic performance evaluation of the designed DAB converter using advanced simulation tools, primarily MATLAB/Simulink. The chapter is divided into several sections, each focusing on different aspects of the converter's performance under varying conditions. Initially, the simulation setup is described, including the configuration of the converter, grid integration, and vehicle load profiles. The chapter then presents detailed simulation results, analyzing performance metrics such as efficiency, switching losses, conduction losses, and thermal performance. The impact of different modulation techniques, such as phase-shift modulation, on the converter's efficiency and power density is evaluated. Furthermore, the chapter explores the converter's behaviour under extreme scenarios, such as high load conditions and fluctuating input voltages.

- Experimental Validation and Hardware Implementation:

  In this chapter, real-world implementations were emphasized. The chapter begins by describing the hardware setup used for validating the simulation results, including the design and assembly of a physical DAB converter prototype. The chapter provides an in-depth discussion of the experimental procedures, including the measurement techniques used for evaluating power semiconductor losses, conduction losses, and overall system efficiency. The hardware results are then compared with the simulation outcomes, highlighting any discrepancies and their possible causes. The chapter also addresses the challenges encountered during the experimental phase, such as thermal management and circuit stability, and discusses the solutions implemented to overcome these issues. The successful experimental validation of the converter's performance confirms the feasibility and effectiveness of the proposed design.

- Conclusion and Future Work:

The final chapter summarizes the key findings of the research, highlighting the contributions made to the field of power conversion for electric vehicle charging and V2G applications. It discusses the implications of the research for the future development of EV infrastructure, particularly in terms of enhancing the efficiency and scalability of charging systems. The chapter also identifies the limitations of the current study and suggests areas for future research, such as exploring alternative converter topologies, improving thermal management techniques, and further enhancing the converter's performance in V2G applications. The potential for integrating the developed technologies with emerging trends in renewable energy and smart grids is also discussed, providing a forward-looking perspective on the impact of this research.

1.4. Single-Stage Topologies

Single-stage topologies found in the literature can be categorized under the following subheadings:

- Non-resonant dual-bridge converters
- Single-stage resonant dual-bridge converters
- Multi-stage resonant dual-bridge converters

Separately, isolated cross, forward, and Cuk converters that are capable of bidirectional operation are usually suitable for applications with output powers below 2 kW. The main advantage of the cross and forward converter structures is their simplicity and the small number of switching components required. However, the ineffective use of transformers and switches in these topologies makes them unsuitable for meeting specific requirements, such as efficiency and high-power compatibility, as discussed in [5].

Non-resonant dual-bridge converter topologies contain more switches and includes full-bridge, half-bridge, or push-pull topologies, which are discussed at [5-8]. Some of the structures in this group are non-resonant. In the non-resonant structures, a series inductor is either added to the transformer's leakage inductance, or the transformer's leakage inductance is utilized directly. Compared to cross and forward converters, converters in this group enable more efficient use of converters. Semiconductor switches operate with fewer switching losses, thus achieving higher power density with these topologies. The most popular structure in this group is the bidirectional full-bridge DC-DC converter and the DAB configuration, which is also presented in [9].

The resonant dual-bridge converters contain resonant topologies with resonant high-frequency structures. These structures can achieve lower switching losses, as introduced in [10]. They also increase complexity and require additional power components.

Topologies can be classified based on the impedance connected directly to the DC terminal. If a capacitor is used, the terminal acts as a voltage source. If an inductor is used, the terminal is considered as a current source [11].

In single-stage topologies, the following six topologies are commonly used and preferred:

- Single-phase DAB Converter
- Three-phase DAB Converter [9]
- LLC Converter [7]
- Bidirectional and isolated full-bridge converter [11]
- Bidirectional and isolated current-doubler topology [12]
- Bidirectional and push-pull topology [11]

1.5. Single-Phase Dual Active Bridge Converter

The single-phase DAB converter is depicted in Figure 2. This topology consists of two full-bridge circuits and a high-frequency transformer. The reactive structure simply comprises an L inductor connected in series with the high-frequency (HF) transformer, where L is derived from the transformer's leakage inductance. Due to its symmetrical structure, the DAB converter easily facilitates bidirectional power flow.

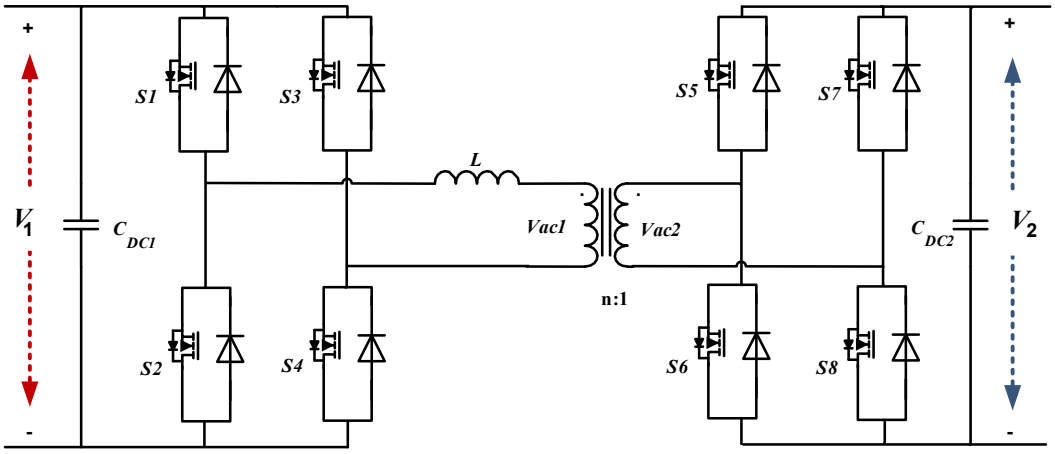

Figure 2. DAB Converter Topology

The primary advantage of this circuit is the low number of passive components it includes and its capability for soft switching, which results in low switching losses. However, soft switching cannot be achieved under low load conditions in DAB converters. Despite this, it is possible to achieve high power density with the DAB converter topology.

Nevertheless, the waveforms of the transformer primary and secondary currents are directly dependent on V_1, V_2, and the output power P_{out} operational points, leading to very high transformer RMS currents at some operational points. In addition, in this topology, the input-output capacitor RMS currents are very high. To mitigate the high RMS currents in the transformer and capacitors, modulation techniques other than the traditional phase shift modulation technique must be used [8].

As a result of the traditional phase shift modulation technique, the switches on the low voltage (LV) side have a low VA rating. Moreover, a low VA rating allows for a high-frequency transformer with low magnetic energy storage capability. This topology has a very low number of inductances, making the high CDC_2 capacitor RMS currents on the LV side challenging for practical circuit realization. The circuit consists of a full-bridge converter on both the high voltage and low voltage sides.

In the literature, some DAB converters also use half-bridge or push-pull structures. For the following reasons, the full-bridge converter structure is the most suitable:

- Only the full-bridge structure can produce a zero-output voltage (voltage applied to the high-frequency structure), allowing for the use of advanced modulation techniques.

- Using a half-bridge reduces the number of switches in the circuit, thereby reducing the number of gate drive circuits in the practical circuit. However, when using a half-bridge, the RMS current values of the switches in the full bridge are doubled. The amplitude of the AC voltage in the half-bridge is half that of the full bridge, which is a significant disadvantage for the LV side. If the half-bridge operates on the LV side, high transformer RMS currents and high switch RMS currents occur.

- When using a push-pull structure, two transformer windings are required. Due to each winding carrying current separately during each half-switching period, the use of the high-frequency transformer becomes inefficient. The transformer VA rating increases. However, using two switches on the LV side and reducing the number of gate drive circuits are advantages. The current values of the switches are the same as in the full-bridge structure, but the switch voltage values are double. Therefore, the VA rating is roughly the same for both the full-bridge and push-pull circuits. A comparative analysis of the two circuits is presented in [4].

1.6. Three-Phase Dual Active Bridge Converter

This topology comprises three half-bridge circuits on the high-voltage side and three half-bridge structures on the low-voltage (LV) side, necessitating three converter inductances and three high-frequency transformers. The three-phase DAB converter, shown in Figure 3, is driven using a modulation technique similar to that of the single-phase DAB converter [9]. However, unlike the single-phase topology, it is not advisable to use performance-enhancing methods in the modulation technique of this topology.

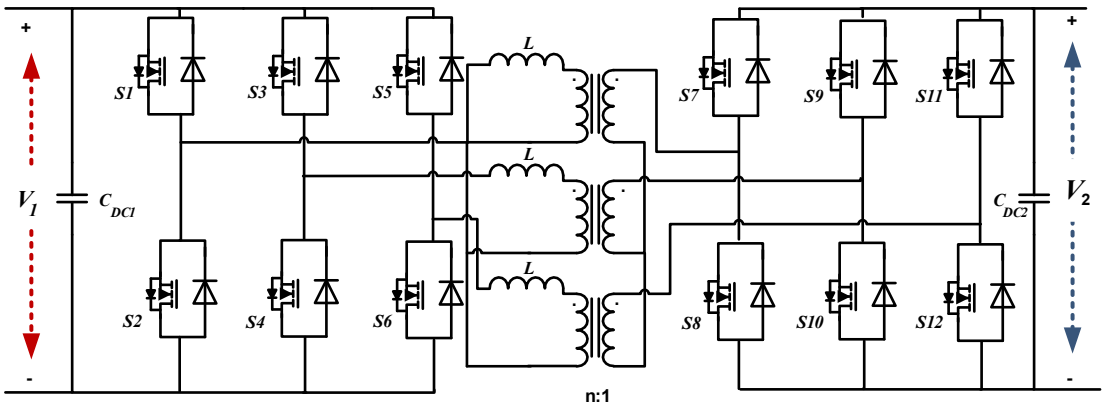

Figure 3. Three-Phase DAB Converter Topology

The three-phase DAB converter achieves good performance with advantages including low VA transformers, low VA switches, and low magnetic energy storage capability. Compared to the single-phase DAB converter, lower capacitor RMS current values can be achieved. According to Figure 3, a disadvantage of this topology is the need for a high number of active components: 12 semiconductor switches and a total of 12 gate drive circuits, including six for the high side. If the converter operates across a wide voltage and power range, high conduction and switching losses occur at certain operating points due to the inability to improve the traditional modulation technique.

1.7. Bidirectional & Isolated Full-Bridge

The bidirectional and isolated full-bridge converter topology is presented in Figure 4. The circuit consists of voltage source full-bridge structures on both the high-voltage and LV sides, using an LDC_2 DC link inductor. The power flow is controlled by the duty cycle D. To allow bidirectional flow, the LV side must be appropriately controlled [13].

In the bidirectional and isolated full-bridge converter, switches on the high-voltage side are switched at zero voltage, while zero current switching technique is used for the switches on the LV side. Operating at high switching frequencies and achieving high power density are suitable for this topology. However, extra circuits are needed at lower power levels.

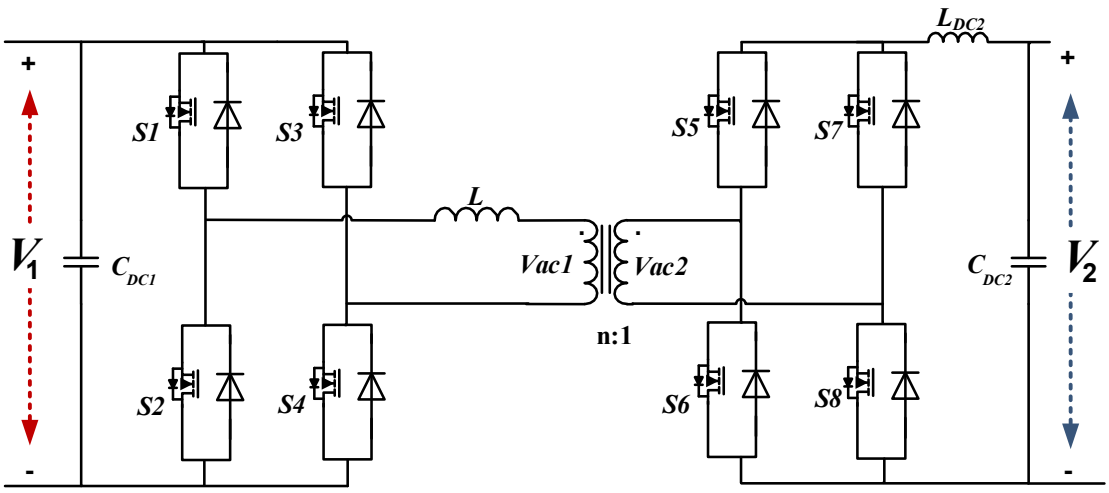

Figure 4. Bidirectional and Isolated Full Bridge Converter Topology

Unlike DAB and LLC converters, the transformer turn ratio utilization values are limited. An extra circuit is required when the system is intended to operate with $V1 \leq nV2$ at startup. The VA ratings of the switches on the LV side in the isolated bidirectional full-bridge converter are higher compared to those in DAB and LLC topologies. This converter achieves a smoother LDC_2 current and lower CDC_2 capacitor RMS current compared to the DAB converter. The major disadvantage of this topology is the need for extra space for the DC inductance LDC_2.

Moreover, since the LV switches, DC inductance LDC_2, and transformer leakage inductance are connected in series, a damping circuit is needed to prevent voltage spikes during switching.

Different topologies are also used on the LV side in the literature, including current-doublers or push-pull structures. Circuits that use a current-doubler structure on the LV side are shown in Figure 5 and the push-pull structure in Figure 6. The advantages and disadvantages of the three different structures on the AC side, namely the full-bridge, current-doubler, and push-pull structures, are as follows:

- The current values of the switches and the total VA values of the switches are similar for all three structures.

- The full-bridge structure has the highest transformer current iAC2 value (both instantaneous and RMS).

- In the current-doubler structure, two inductances are required instead of one, leading to a slightly higher total magnetic energy storage capacity due to reduced ripple. However, the values of iLDC2a and iLDC2b are high, resulting in an increased transformer VA value. Compared to the full-bridge structure, twice the transformer voltage, vAC2, is needed, which achieves a lower iAC2 transformer current. The current-doubler structure requires two AC-side switches, and the voltage across these switches is twice that of those in the full-bridge.

- The push-pull circuit uses a center-tapped transformer on the AC side with two transformer windings. Each half-switching cycle utilizes these windings separately, making transformer use inefficient and leading to high VA values. The voltage across the two AC-side switches in the push-pull topology is the same as in the full-bridge.

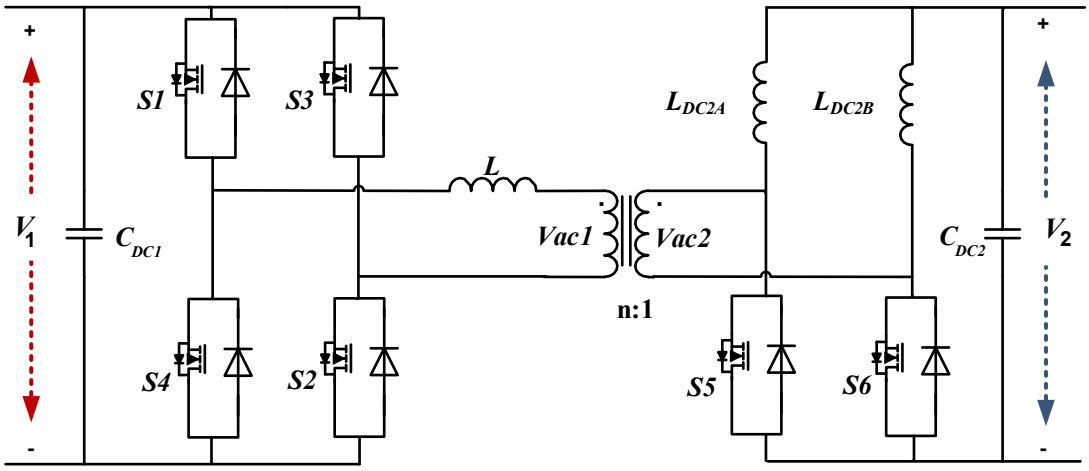

Figure 5. Bidirectional and AC-Side Isolated Current-Doubler Structure

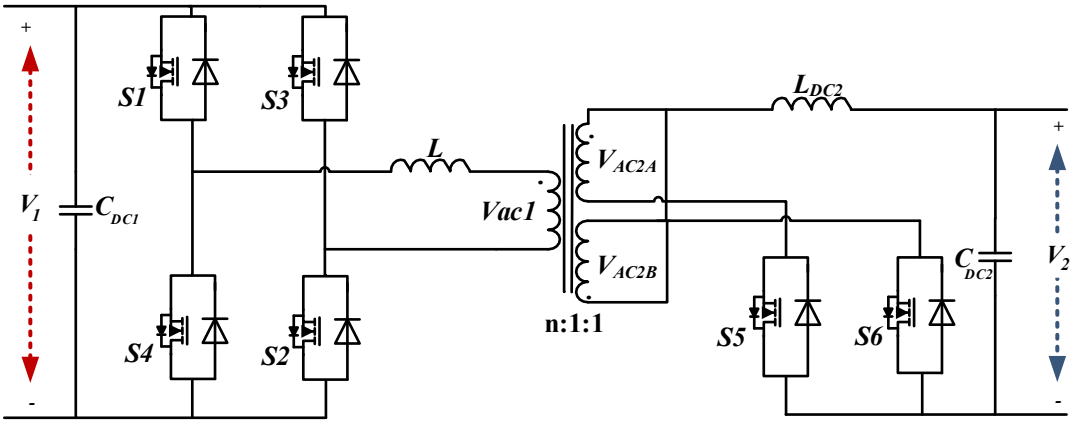

Figure 6. Bidirectional and AC-Side Isolated Push-Pull Structure

1.8. Other Non-Resonant Converter Topologies

The literature has explored DC-DC converters with a minimum number of components [14]. A bidirectional DC-DC converter topology with a minimum number of switches is shown in Figure 7. It uses a voltage-source half-bridge on the DC side and a modified half-bridge structure on the AC side. The topology is a DAB converter with a half-bridge on the AC side.

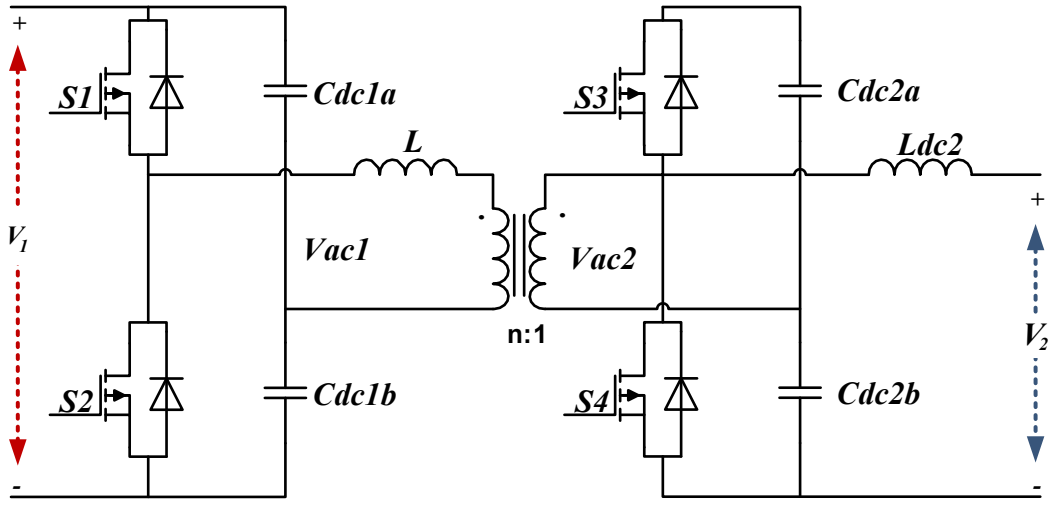

Figure 7. Bidirectional DC-DC Converter with a Minimum Number of Switches

This structure can be used bidirectionally as either a step-down or step-up converter. Similar to the traditional DAB converter, the transferred power is controlled by the phase shift between v_{AC1} and v_{AC2}. This converter results in unequal RMS switching currents for S3 and S4 and a high maximum withstand voltage. The capacitor on the AC side has a high RMS current value, similar to the DAB converter. The optimum efficiency modulation technique applied in the DAB converter due to the half-bridge structure cannot be used here. However, asymmetric PWM waveforms can be generated to adjust V2, which allows for optimization of the converter. The limited soft-switching capability, high capacitor RMS currents, and the additional need for DC inductance make this circuit less preferred in applications.

In the literature, modifications to the AC side of this circuit have been made, implementing a current-doubler circuit on the AC side with a voltage-source half-bridge circuit on the DC side [15]. Power transfer was controlled using an asymmetric pulse width modulation technique. However, this structure also results in high current stress values across all power components.

1.8.1. Resonant Dual Bridge Converters

Although there are numerous unidirectional DC-DC resonant converters in the literature, there are very few bidirectional resonant converters. This is due to increased circuit complexity and the need for additional high-frequency components. Series, parallel, and series-parallel resonant topologies are the most popular unidirectional resonant topologies [15], [16]. These converters achieve nearly sinusoidal transformer current waveforms, enabling low switching losses and allowing the converter to operate at high power values and high switching frequencies. Traditional resonant DC-DC converters operate at variable switching frequencies, which change according to input voltage and load.

1.8.2. Other Resonant DC/DC Converters

Different from SRÇ (Series Resonant Converter), PRÇ (Parallel Resonant Converter), and SPRÇ (Series-Parallel Resonant Converter) topologies, the literature includes bidirectional resonant converters [16]. These feature a voltage-source half-bridge structure on the DC side and a full-bridge structure with quarter-bridge switches on the AC side, effectively changing the resonant capacitor value. This configuration achieves high efficiency across a wide load range. In [15] and [16], the switching frequency is reduced under low load. However, the AC side voltage V2 cannot exceed V1/n. A different modulation technique achieves transformer current waveforms similar to those of the LLC converter, but with a higher VA value for this converter.

Another approach in the literature is to achieve lower switching losses with a resonant converter by reducing the values of CDC_1 and CDC_2 in the DAB converter [17]. This requires designing an additional electromagnetic interference (EMI) filter. Due to its complexity and the generation of high RMS currents, this configuration is difficult to implement.

2. Two-Stage Topologies

B. Muhammetoglu[1], M. Jamil[2]

[1,2] Electrical and Computer Engineering Department, Faculty of Engineering and Applied Sciences, Memorial University of Newfoundland, St. John's, Canada

A version of this manuscript chapter has been presented at the 2024 12th International Conference on Smart Grid (icSmartGrid), Setubal, Portugal. As the primary author, B. Muhammetoglu conducted the research under the guidance of M. Jamil, who served as the co-author. B.M. was responsible for performing the literature review, system selection, design, calculations, simulations, and efficiency evaluations. The co-author contributed by refining the research concepts and providing critical feedback and revisions to the manuscript. Additionally, the paper earned the "Best Paper Award" among all the papers presented at the conference.

Published Reference: B. Muhammetoglu and M. Jamil, "Design and Optimization of a Scalable Bidirectional DC-DC Converter for Electric Vehicle Charging Applications using SiC Switches," 2024 12th International Conference on Smart Grid (icSmartGrid), Setubal, Portugal, 2024, pp. 423-428, doi: 10.1109/icSmartGrid61824.2024.10578205. Keywords: Silicon carbide, Bridge circuits, DC-DC power converters, Electric vehicle charging, Distance measurement, Smart grids, Batteries, Electric Vehicle (EV), Bidirectional Power Converter, Vehicle-to-Grid (V2G), Dual Active Bridge (DAB), Dual Output Converter, Silicon Carbide (SiC)

Published Reference Link: https://ieeexplore.ieee.org/document/10578205

The most efficient operation of isolated DC-DC converters occurs when the V1/V2 ratio is close to the turn ratio, n. Therefore, using a two-stage topology allows for the application voltage to the isolated DC/DC converter to be adjusted by adding an extra step-down and/or step-up stage. However, two-stage converters require a large number of power components. The efficiency of the added non-isolated converter stage must be very high; otherwise, it cannot surpass the efficiency value of the single-stage converter.

Two-stage topologies have been examined as follows, with a step-down converter on the DC side, a step-up converter on the DC side, a step-down converter on the AC side, and a step-up converter on the AC side:

- Using a step-down converter structure on the DC side reduces the input voltage to the isolated bidirectional converter. This allows for the selection of switches with lower voltage ratings, but results in higher current values. Generally, this structure achieves an efficiency of around 90%.

- When a step-up converter is used on the DC side, the voltage coming to the DC side is higher than the DC bus voltage. Since it is difficult to find high-efficiency MOSFET switches for applications above 600 V, the increased voltage value must be carefully chosen when using this topology.

- Using a step-down converter on the AC side allows for lower current on the AC side of the isolated bidirectional converter. However, achieving a high-efficiency, low-voltage, high-current output step-down converter is challenging [18].

- With a step-up converter on the AC side, the DC bus voltage is lower than the output (V1<V2). Therefore, the current amplitude in the isolated AC side switches and the HF transformer increases. This structure is not suitable for high-efficiency operation.

Bidirectional buck-boost type converters can also be used in these circuits, but they are less preferred due to requiring more switches. The advantages and disadvantages of single-stage, bidirectional, and isolated DC/DC converter topologies are summarized below:

- DAB (Dual Active Bridge) Converter: It contains only one inductance L and has a low peak energy storage capacity. It features low VA value semiconductor switches on both the DC and AC sides. Preferred for its zero-voltage switching [19], [20] and capability to employ various modulation techniques. Due to its symmetrical structure, the efficiency of the converter is independent of the power transfer direction. The disadvantages of the DAB converter include high RMS current values of the CDC2 capacitor, high transformer winding currents on the AC side, and the need for a complex modulation algorithm to generate gate signals.

- Three-Phase DAB Converter: Advantages include a low VA value transformer, low VA value switches, low peak magnetic energy storage capacity, zero-voltage switching, low RMS current value of the CDC2 capacitor, and a symmetrical structure. However, the disadvantage is the need for numerous components (3 transformers, 3 inductances, 12 switches), making this circuit's efficiency lower than that of the single-phase DAB converter and the LLC converter.

- LLC Converter: Compared to the DAB converter, the efficiency is slightly higher. The VA values of the semiconductors are similar. However, the need for an additional resonant capacitor for the resonant circuit and a high magnetic storage requirement are disadvantages, making it larger in size compared to the DAB converter. The RMS current value of the CDC2 capacitor is also high in this topology.

- Full-Bridge Converter: The switches on the DC side are switched at zero voltage, and zero-current switching is used for the switches on the AC side. The RMS current value of the CDC2 capacitor is low in this topology. However, unlike DAB and LLC converters, the transformer turn ratio utilization values are limited. An extra circuit is needed when the system starts operating with $V1 \leq nV2$. The semiconductor switches have a high VA value, and there's a need for a DC inductor.

In all single-stage converter topologies, the VA value of the HF transformer is similar, and the volumes of the transformers are comparable.

2.1. Series/Parallel and Interleaved Topologies

In automotive applications, due to the voltage difference between the DC side and the AC side, the DC side is usually connected in series, while the AC side is connected in parallel. The series connection allows for the use of silicon MOSFETs with low breakdown voltage. On the AC side, paralleling is done both to meet the high current demand and to reduce the conduction resistance of the semiconductors. When silicon carbide MOSFETs are used on the DC side, there's no need for series connection.

However, paralleling on the AC side is necessary to achieve high power levels and minimize conduction losses. In interleaved operation, triggering the AC side switch groups with a phase shift reduces both the current stress on the switches and the effective value and size of the output filter elements.

In this research, a design for a DAB converter that allows bidirectional power flow with galvanic isolation, high efficiency, and high-power density compared to similar isolated bidirectional converter topologies has been selected and tested.

Silicon carbide power MOSFET semiconductors were used on the high voltage side, and silicon CoolMOS power MOSFET semiconductors were used on the low voltage side. The unique aspects of this converter design include:

- A DAB converter with a main power of 5.6 kW that can be used for both heavy-electric and light-electric vehicles without any change in magnetic circuit elements,

- The capability to easily operate between 3.7 kW and 11.2 kW power levels for different application needs thanks to its interleaved and parallel operating features,

- A high-frequency transformer design with dual secondary outputs and an appropriate thermal design of the printed circuit board, capable of transferring power at the highest current condition of 260 A,

- An optimized efficiency competitive single-stage dual-direction converter design through the use of new generation power semiconductors and relatively low-loss magnetic circuit elements,

- The converter can be easily configured according to the desired power value, vehicle type, and application need, and its capability for bidirectional power transfer offers the potential for future applications (such as Vehicle-to-Grid). This design is compared to various different designs discussed, and the following results were obtained:

Table 1. Comparison with Different State-of-the-art EV Chargers

Parameters	[21]	[22]	[23]	[24]	[25]	[26]	[27]	Proposed
Power(kW)	0.5	1.5	32	7.5	7	33	20	3.7-11.2
Voltage(V)	110	140	220	450	450	500	750	450-750
Frequency (kHz)	20	50	20	67	120	200	350	50
# of Active Components	6	6	8	10	12	10	20	6-8
***η* (%)**	>93	~96	~97	97	>95	96	97	97(F.L.)-98(H.L.)

2.2. Modes of Operation for DAB Battery Charger

The advantages of the DAB, such as its ability to transfer power bidirectionally, perform soft switching over a wide voltage range, operate with numerous modulation techniques, and achieve high efficiency, make it an appealing choice for battery charging converters in both heavy and light electric vehicles. This study proposes a low-voltage battery charger converter for both heavy and light electric vehicles, utilizing a DAB topology with silicon carbide and silicon switches. The combined use of silicon carbide and silicon switches results in a highly efficient, high power density, and compact converter.

Two different converter configurations, each based on the main power structure of a 5.6 kW DAB converter, are illustrated in Figure 8-9. As shown in figures, the proposed converter can be used in various power values and applications. The nominal input voltage, output voltage range, and power values for the converters in Figure 9 are provided separately on the figure. For heavy electric vehicles, a battery charger converter powered by a high voltage battery ranging from 400-900 V and capable of 11.2 kW is shown in Figure 8.

The converter operates by interleaving two parallel DAB converters, each of 5.6 kW. It is designed to charge two series-connected 12 V batteries within a range of 16-32 V with a maximum output current of 200 A. On the other hand, the main 5.6 kW DAB converter is configured to be powered by a vehicle battery in the range of 250-400 V and to operate as a battery charging converter for light electric vehicles with a maximum power of 3.7 kW. In this scenario, the DAB converter will charge a single 12 V battery with a maximum output current of 260 A in the voltage range of 8-16 V. Both configurations can use a single DAB converter without any updates to the semiconductor power switches or magnetic circuit elements.

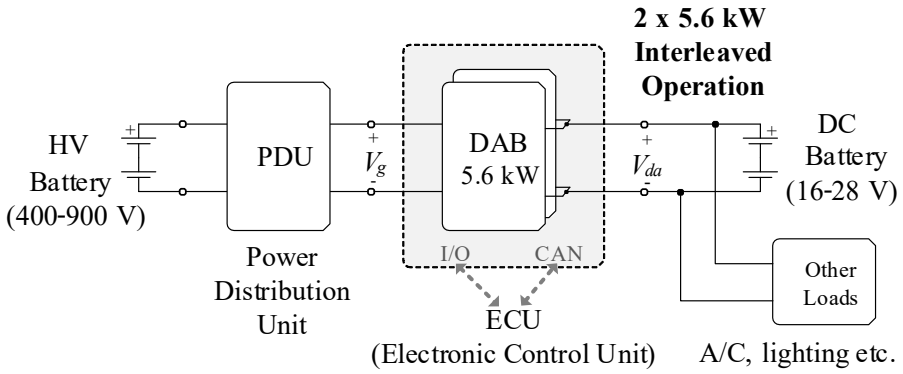

Figure 8. 11.2 Kw Battery Charger Converter for Heavy Electric Vehicles

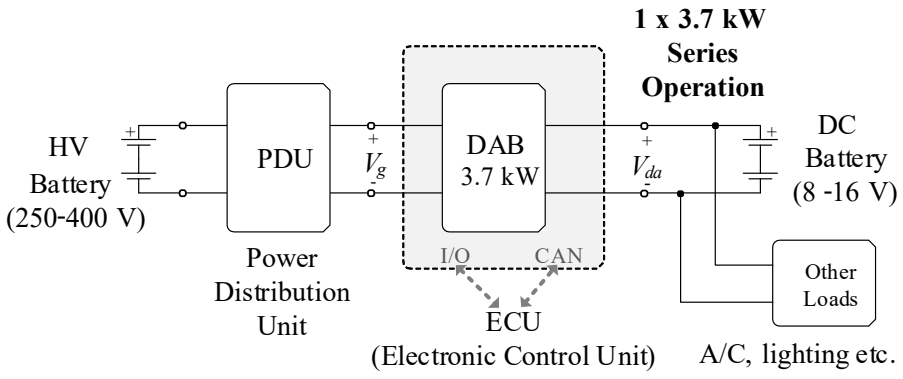

Figure 9. 3.7 Kw Battery Charger Converter for Light Electric Vehicle

PWM signal used for the CC/CV charging is generated through the comparison of a square wave carrier with a constant signal, which is indicative of the duty cycle. This duty cycle signal is dynamically adjusted in response to our reference parameters.

Employing a Zero Current/Voltage Switching (ZCS/ZVS) methodology, the reference for this converter aligns with the active power provided to the AC/DC converter, ensuring synchronization between the two signals. When designing filters for AC-DC PWM converters, it's important to consider various factors such as the ripple in the line current, the size of the filter, and the effectiveness in reducing switching ripples. The inductance on the converter side, denoted as L_i, can be calculated using the formula presented in the equation:

$$L_i = \frac{V_{DC}}{16\, f_s\, \Delta I_L} \tag{1}$$

In this equation, f_s represents the switching frequency of the converter, and ΔI_L is the ripple current of the line inductor.

The converter's switching frequency is denoted as f_s, and ΔI_L symbolizes the ripple current of the line inductor. Typically, the ripple current in the inductor on the converter side, ΔI_L, is selected to be 10% of the phase current. Consequently, the formula for ΔI_L can be articulated as follows: The ripple current ΔI_L is given by the equation:

$$\Delta I_L = 0.1\sqrt{\frac{2P_{ph}}{V_{ph(\mathrm{grid})}}} \tag{2}$$

where P_{ph} represents the nominal power of the converter per phase, and $V_{ph(grid)}$ is the RMS value of the single-phase grid voltage.

For the grid-side inductances $L_{R\text{-}Y\text{-}B}$, a suitable value can be determined using $L_{R\text{-}Y\text{-}B} = 0.6L_i$. In addition, the filter capacitance C_F should be set to 5% of the base capacitance C, as per the formula:

$$C_F = 0.05C = \frac{P_{ph}}{\omega_{grid} V_{ph(\mathrm{grid})^2}^2}, \tag{3}$$

where ω_{grid} is the grid's rotational frequency.

The resonance frequency of the designed LCL-filter is calculated using:

$$f_o = \frac{1}{2\pi}\sqrt{\frac{L_i + L_g}{L_i L_g C_f}} \quad (4)$$

Additionally, to enhance the filter's performance, an Equivalent Series Resistor R_{EQ} can be added in series with the battery capacitor C_{DC2}/C_F, as depicted in Figure 2. The value of the damping resistor, R_{EQ} is determined using the following equation:

$$R_B = \frac{1}{6\pi f_0 C_f} \quad (5)$$

Additionally, an LCL-filter is employed on the grid side of the three-phase bidirectional EV charger, serving the purpose of reducing line current harmonics. The real-time signal delivered to the battery is monitored, and any discrepancy between this actual signal and the reference signal—essentially the error signal—is processed through the control system.

The controller's output determines the necessary duty cycle, which is then compared to the carrier to generate appropriate switching signals for the Insulated Gate Bipolar Transistors (IGBTs).

If the measured current/voltage falls below the reference, resulting in a positive error, the duty cycle is increased to compensate. Conversely, a higher actual current/voltage than the reference, indicating a negative error, leads to a reduction in the duty cycle. This control mechanism inherently produces oscillations around the target value. To mitigate this and to ensure the emission of a clean waveform, DC-link components incorporated are utilized to filter out harmonics.

3. Alternative Power Stage Connections

B. Muhammetoglu[1], M. Jamil[2]

[1,2] Electrical and Computer Engineering Department, Faculty of Engineering and Applied Sciences, Memorial University of Newfoundland, St. John's, Canada

A version of this section of the manuscript chapter has been accepted by the Smart Grids and Microgrids Journal with minor revision. B. Muhammetoglu conducted the research under the guidance of M. Jamil, who served as the co-author. B.M. was responsible for performing the literature review, system selection, design, calculations, simulations, and efficiency analysis. The co-author contributed by refining the research concepts and providing critical feedback and revisions to the manuscript.

Reference: • Muhammetoglu, B.; Jamil, M. DAB Converter with Interleaved and Parallel Operation for Electric Vehicle Charging. Energies 2024, 17, 4258. https://doi.org/10.3390/en17174258 , Published

3.1. Alternative Power Stage Connection-1 for 11.2 kW Heavy-Vehicle Converter

This configuration achieves operation by paralleling two 5.6 kW units and operating them in an interleaved manner, with the general block diagram provided in Figure 10. To optimize efficiency and maintain the temperatures of the MOSFETs on the AC side within appropriate ranges, three parallel MOSFETs are used. Thus, for a single 5.6 kW unit on the AC side, 12 MOSFETs are used, totalling 24 MOSFETs for the 11.2 kW converter. Each 5.6 kW unit uses a transformer with a single primary and a single secondary output.

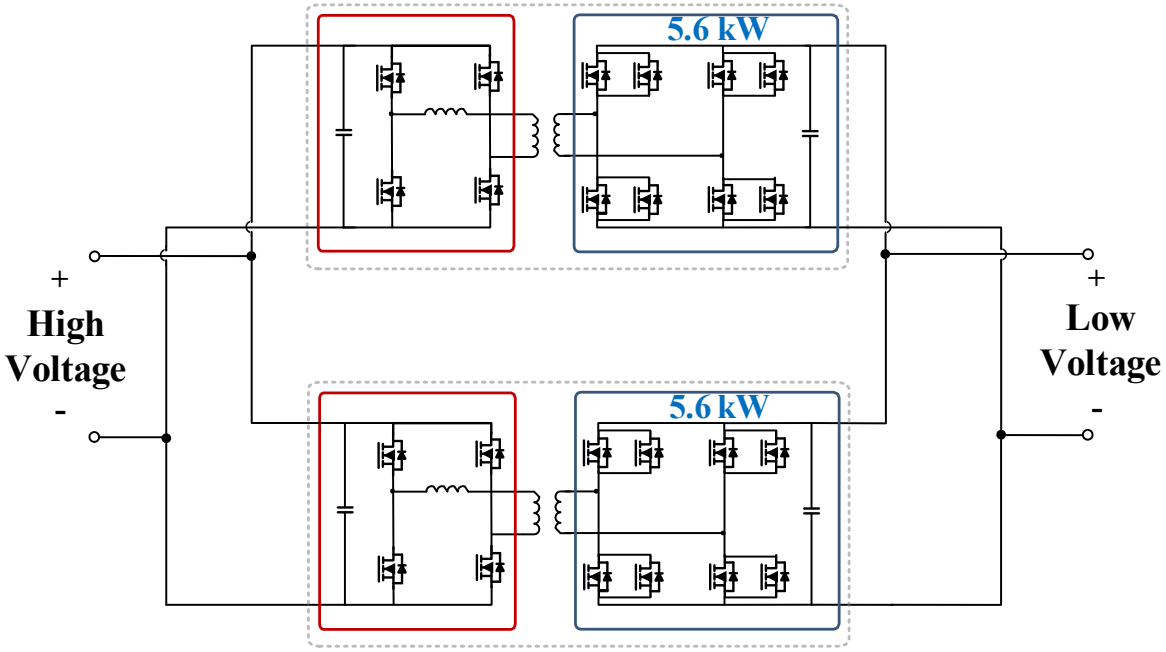

Figure 10. Alternative Unit Connection-1 for The 11.2 Kw Heavy-Vehicle Converter

Interleaved operation reduces the ripple current of the output capacitor, subsequently decreasing the capacitor's value. The disadvantages of this alternative include the use of 24 MOSFETs, potential current sharing issues among parallel MOSFETs, the challenge of driving parallel MOSFETs, and the difficulties in PCB design due to effective currents of 200 A passing on the secondary side of the transformer for each 5.6 kW unit.

3.2. Alternative Power Stage Connection-2 for 11.2 kW Heavy-Vehicle Converter

In this connection, each 5.6 kW unit's transformer secondary output is doubled, designed to provide 2.8 kW per output, with the block diagram shown in Figure 11. Since there is no need for paralleling in each 2.8 kW unit, only one MOSFET is used. Consequently, 8 MOSFETs are used on the AC side for each 5.6 kW unit, totaling 16 MOSFETs. This alternative uses 8 fewer MOSFETs compared to the other option. The 2.8 kW units are paralleled among themselves, while the 5.6 kW units operate in an interleaved manner.

The transformer used in this alternative has dual outputs, reducing each output's secondary current to around 100 A, facilitating easier PCB design. Although the effective currents through the MOSFETs have increased compared to the previous alternative, they remain within normal operating limits.

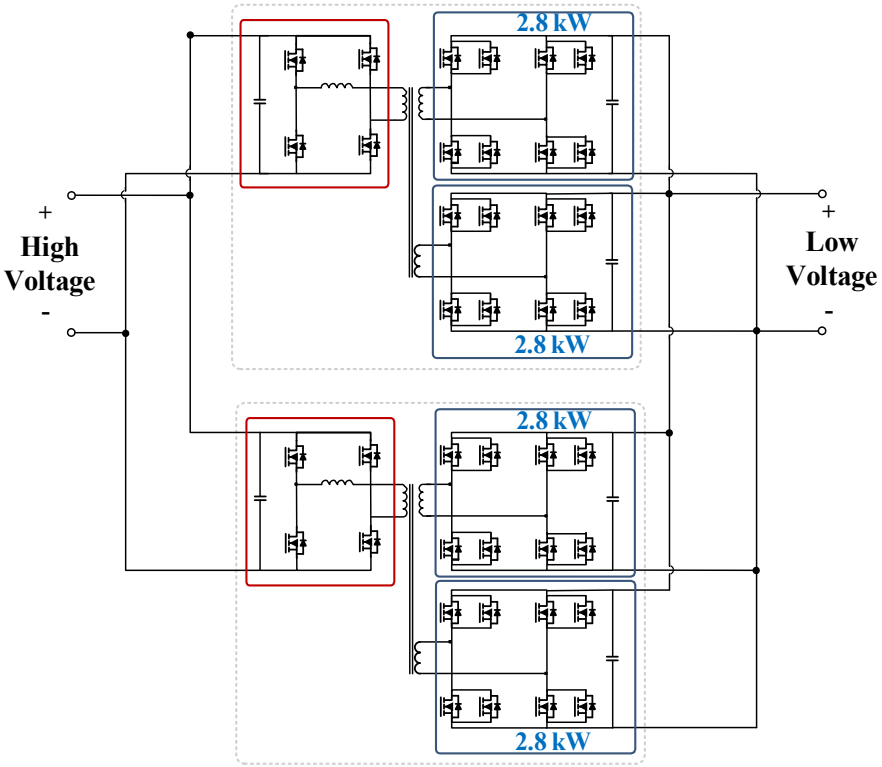

Figure 11. Alternative Unit Connection-2 for the 11.2 kW Heavy-Vehicle Converter

The interleaved operation of the 5.6 kW units maintains the same output ripple currents as the previous alternative. The reduced number of MOSFETs, ease of driving, and simpler PCB design make this alternative more feasible. Dual-output secondary of the transformer is possible, however may complicate the design.

3.3. Power Stage Connection for 3.7 kW Light-Vehicle Converter

In this connection, the 3.7 kW converter's output power is achieved by parallel operation of two 1.85 kW output stages. To reach the targeted efficiency and ensure the temperatures of the AC-side MOSFETs remain within appropriate ranges, 2 parallel MOSFETs are used. Thus, for the 3.7 kW unit, 16 MOSFETs are utilized on the AC side. Each 2.7 kW unit on the AC side will operate at a peak of 1.85 kW at full power. Since the DC side is single, interleaved operation is not possible; hence, the AC side operates in parallel.

The technical specifications of each converter (for heavy and light electric vehicles) shown in Figure 8-9 are provided separately in Table 2.

As previously mentioned, the main power stage, a 5.6 kW DAB converter, can be used for both an 11.2 kW heavy electric vehicle, operating in phase-shifted mode, and a 3.7 kW light electric vehicle charger, by merely changing the energy transfer inductor of the magnetic circuit elements.

Table 2. HF Transformer Design Specifications

Technical Specification	***Output 1***	***Output 2***
Nominal Input Voltage (V)	750	400
Nominal Output Voltage (V)	28	14
Nominal Output Current (A)	200	260
Nominal Output Power (kW)	5.6	3.7
Switching Frequency (kHz)	50	
Transformer Turn Ratio (n)	30:1:1	
External Inductor Value (μH)	70	
Output Capacitor (mF)	7.2	
Output Capacitor ESR (mΩ)	3.6	

The main power board of the DAB converter is designed with a circuit board that can transfer power smoothly under the highest current condition of 260 A. The circuit of the main 5.6 kW DAB converter is given in Figure 12.

For the high voltage side, which is the input H-bridge circuit of the DAB converter, silicon carbide power MOSFET switches are used instead of silicon-based power MOSFET switches due to their superior low switching losses, high thermal stability, and high breakdown voltage. The use of silicon carbide switches allows the DAB converter to operate at a higher switching frequency, thereby reducing the size of passive and magnetic circuit elements in the circuit and increasing the power density of the converter. Moreover, the low output capacitors (Coss) of silicon carbide switches reduce the energy required for soft switching, making soft switching easier to achieve.

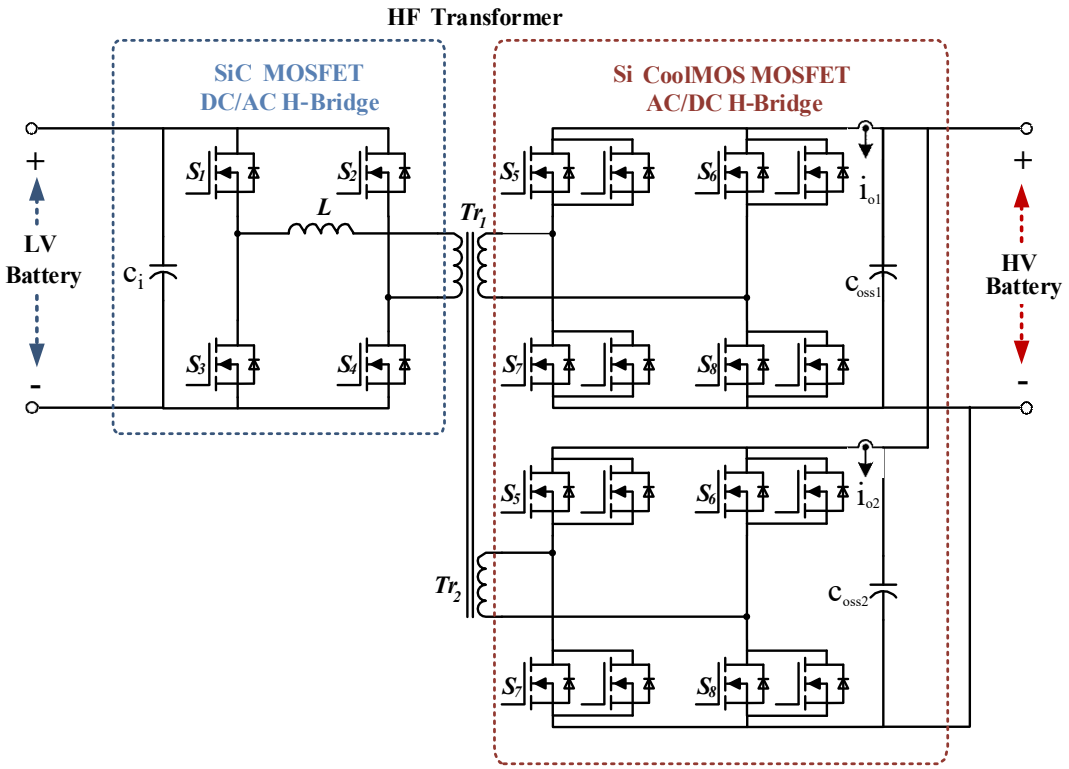

Figure 12. Main Circuit Diagram of the 5.6 Kw DAB Converter.

On the other hand, silicon-based power MOSFET switches are used in the output stage of the DAB converter due to the low voltage on the secondary side. The conduction losses of the switches are dominant due to the high current on the secondary side. At this stage, the conduction resistances of silicon-based power semiconductors are lower compared to other switches, optimizing the design. To theoretically stay within a thermally safe range and further reduce the conduction resistance, the silicon-based switches in the H-bridge circuit of the output stage are used in pairs in parallel. The parallel H-bridge circuits on the secondary side of the DAB converter share the current equally under normal operating conditions. If equal current sharing is not achieved in the output stage H-bridge circuit, unwanted currents will circulate between the bridges, increasing the losses of both the high-frequency transformer and the switches in the output stage, thus leading to thermal issues. The filter capacitors on the input side and the capacitors capable of carrying high RMS currents on the output stage of the DAB converter can be significantly reduced when operating with phase-shifted switching of two 5.6 kW DAB converters.

By nature of the DAB topology, there is no filter inductor on the output, which results in high RMS ripple currents passing through the output capacitors and also high voltage ripples on the output voltage.

This issue can be easily resolved with interleaved switching. For this purpose, the power stage switching of each DAB converter should be phased 180 degrees apart (for two DAB converters). This approach effectively cancels out the high-frequency ripple currents drawn from the input and output power stages, resulting in much lower levels. This, in turn, reduces the RMS current requirement of both input and output capacitors, allowing for the use of commercially smaller capacitors.

3.4. DAB Operation Phases

In the DAB converter topology, power transfer occurs through appropriate phase shifting of the high-frequency square wave between two H-bridges. In its simplest form, these square waves are generated with a D = 1/2 duty cycle, and this method is referred to as single-phase shift (SPS) technique. Power transfer occurs from the leading H-bridge to the lagging H-bridge, and the magnitude and direction of the transferred power can be easily controlled by changing the phase shift parameter.

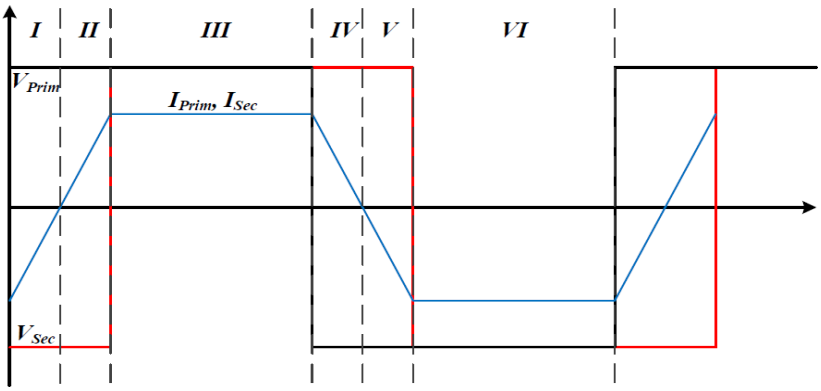

Figure 13. Typical Switching Waveforms for The DAB Converter Using the Single-Phase Shift Method

The power transfer fundamentally occurs through the leakage inductance of the high-frequency transformer or an inductor externally added to the circuit. Due to the phase-shifted nature of the DAB converter topology, the inductor current and voltage follow each other with a certain delay, resulting in unwanted reactive currents circulating within the circuit or between the H-bridges. These currents increase both the current stress on the semiconductor switches and the copper losses in the high-frequency transformer. Advanced modulation methods containing complex control techniques, such as dual-phase shift and triple-phase shift, can significantly reduce this reactive current problem. In this study, the single-phase shift modulation technique has been preferred and used for its ease of application.

The basic operating phases of the DAB converter are presented in Figure 14. For clarity, the switching sequence is examined in six distinct intervals (4 active). The voltage and current waveforms for these intervals are given in Figure 13. In the first interval, the current through the energy transfer inductor changes from a negative to a positive value. During this interval, the primary side switches S1 and S4, and the secondary side switches S6 and S7 are conducting.

The voltage difference between the primary and secondary windings of the transformer is seen across the energy transfer inductor, and the slope of the inductor current during this condition is calculated as shown in Equation 1. Besides the fundamental component of the energy transfer inductor current, high-order harmonic components are present due to the rise or fall times of the current during its increasing or decreasing moments. These high-frequency harmonic components increase the core losses of the inductor.

$$\frac{\mathrm{dI}}{\mathrm{dT}} = \frac{\mathrm{V}_P + \mathrm{V}_S}{\mathrm{L}} \tag{6}$$

In the second interval, the inductor current is entirely positive, and while the primary side switches S1 and S4 continue to conduct, the secondary side switches S5 and S8 start conducting. A zero-voltage switching occurs in the dead-time region of this interval. The slope of the inductor current during this interval is given in the equation below:

$$\frac{dI}{dT} = \frac{V_P - V_S}{L} \tag{7}$$

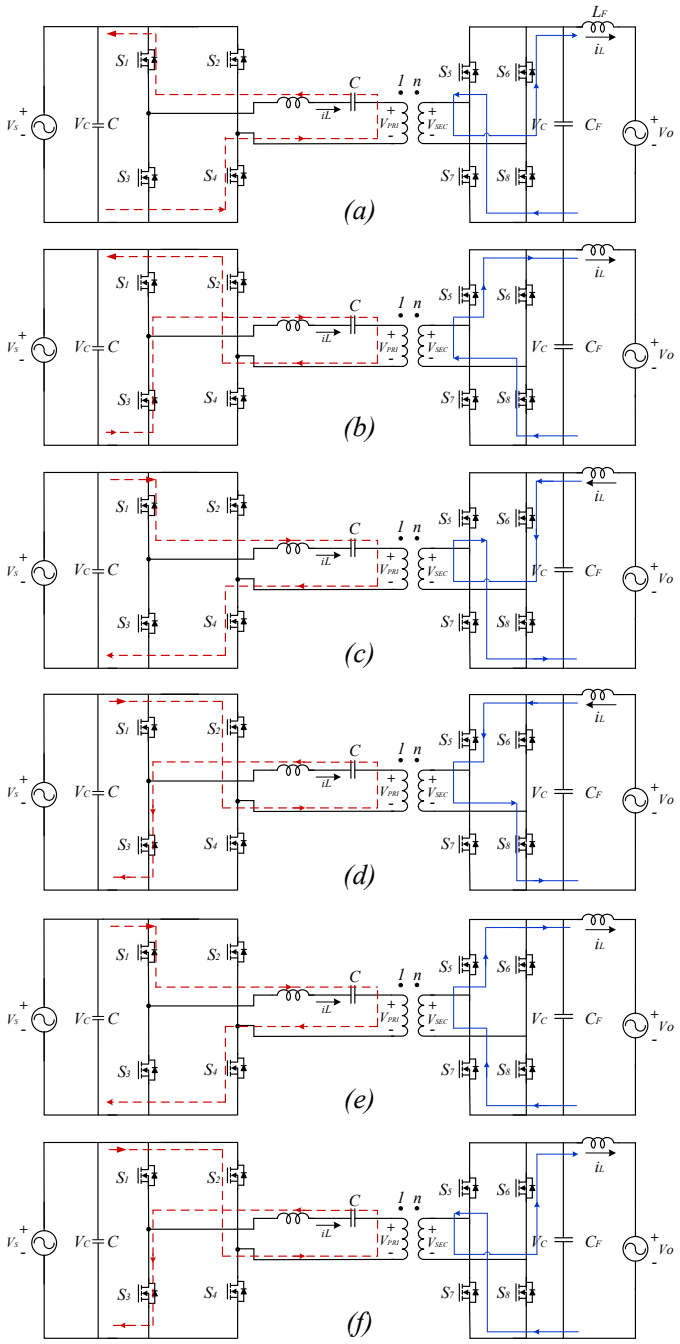

Figure 14. Operating Phases of The DAB Converter - Phases 1-6 (a-f)

In the third interval, the inductor current decreases from its peak value to a negative value. Due to the negative voltage across the inductor in this interval, the inductor current decreases with a slope given in Equation 3.

During this interval, while the secondary side switches S5 and S8 continue to conduct, the primary side switches S2 and S3 start conducting due to the negative voltage across them:

$$\frac{dI}{dT} = -\frac{V_P + V_S}{L} \tag{8}$$

In the fourth interval, the inductor current continues to be negative and decreases with a negative slope as given in Equation 8. During this interval, the primary side switches S2 and S3 continue to conduct, while the secondary side switches S6 and S7, as in the previous interval, start conducting again.

$$\frac{dI}{dT} = -\frac{V_P - V_S}{L} \tag{9}$$

As previously mentioned, during the transition from phase one to phase two, in the dead-time region, the energy charged on the energy transfer inductor discharges the output capacitors of the relevant MOSFETs and maintains their voltage at zero before they start conducting again. This phenomenon is referred to as Zero Voltage Switching (ZVS). One of the greatest advantages of the DAB converter becomes evident here. Due to the nature of the DAB topology, the delayed current stored in the inductor, caused by the phase difference between the two H-bridges, enables all switches in the lagging bridge to perform ZVS, while the switches in the leading H-bridge perform ZVS on one leg under all load conditions. ZVS depends on the load conditions at that moment and hence on the energy stored in the inductor. This allows the output capacitors of the MOSFET switches to be completely discharged.

Another important point is that the MOSFET power switches in the lagging H-bridge operate with synchronous rectification (through the MOSFET's conduction resistance), while the MOSFET power switches in the leading H-bridge, according to the phase shift, mostly operate in forward conduction mode (through the body diode).

4. Design of the DAB Converter

B. Muhammetoglu[1], M. Jamil[2]

[1,2] Electrical and Computer Engineering Department, Faculty of Engineering and Applied Sciences, Memorial University of Newfoundland, St. John's, Canada

A version of this section of the manuscript has been accepted by the ScienceDirect Advances in Electrical Engineering, Electronics and Energy Journal with minor revision. B. Muhammetoglu conducted the research under the guidance of M. Jamil, who served as the co-author. B.M. was responsible for performing the literature review, system selection, design, calculations, simulations, and efficiency analysis. The co-author contributed by refining the research concepts and providing critical feedback and revisions to the manuscript.

Reference: "Two-Stage Variable Voltage AC-DC Converter with High-Frequency DC-Link Isolation for Vehicle to Grid (V2G) Applications," e-Prime - Advances in Electrical Engineering, Electronics and Energy, ELSEVIER

In this section, computer simulation studies of the DAB converter have been conducted, and the operating conditions of the converter have been optimized according to different power levels, input voltages, energy transfer inductor inductance values, and phase shift values between converter voltages, as specified in Table 3. Alongside these studies, switching and conduction losses of the power semiconductors to be used have been obtained through both theoretical calculations and simulation studies, and compared.

The core material and winding design for the energy transfer inductor and the high-frequency transformer to be used in the AC link have been optimized to enhance efficiency. The design of the transformer and inductor has been updated to be used in converters for both configurations, taking into account their current characteristics.
In electric vehicle converter applications, topology selection and power stage design are crucial, but so are volume, weight, and power density. The selection and design of power semiconductor switches and magnetic circuit elements have taken these factors into account to minimize cooling needs and optimize efficiency.

The high-frequency transformer design for use in the AC link has been tailored to operate in both heavy and light electric vehicle converters. The HF inductor design has been separately optimized for each configuration to enhance efficiency. Thus, components that are relatively challenging to design have been made to be commonly used across different configurations as much as possible, while components that are easier to design have been designed separately for different configurations.

4.1. Dual Active Bridge Simulation Studies and Power Semiconductor Loss Calculations

Simulation studies for the 5.6 kW single unit converter, which can be commonly used in both configurations, have been conducted using the MATLAB Simulink program based on the circuit provided in Figure 12. Simulation studies for the DAB topology were first conducted using ideal switches and passive elements, followed by simulations with selections based on real commercial products. To verify the accuracy of the proposed approach, we conducted simulations under various conditions, including extreme battery scenarios and realistic environments described in this section.

These simulations were then utilized with RT-LAB to perform hardware validation using our OPAL-RT system. The simulations were performed using MATLAB version 2022a and RT-Lab 2023.1 on a system running an Intel Core® i7™ 13650HX CPU at 2.6 GHz, with a 64-bit Windows 11 OS and 32 GB of DDR5 RAM clocked at 4800 MHz.

For this study, we utilized the OP5707XG RT-Laboratory from OPAL-RT, a real-time simulator fully integrated with MATLAB. The RT setup consists of two PCs: one as the host and the target PCs, connected via TCP/IP protocol. The OPAL-RT OP5707 XG is equipped with 64 fast Input/Output channels featuring DB37 and RJ45 connectors, with the latter being used in our configuration.

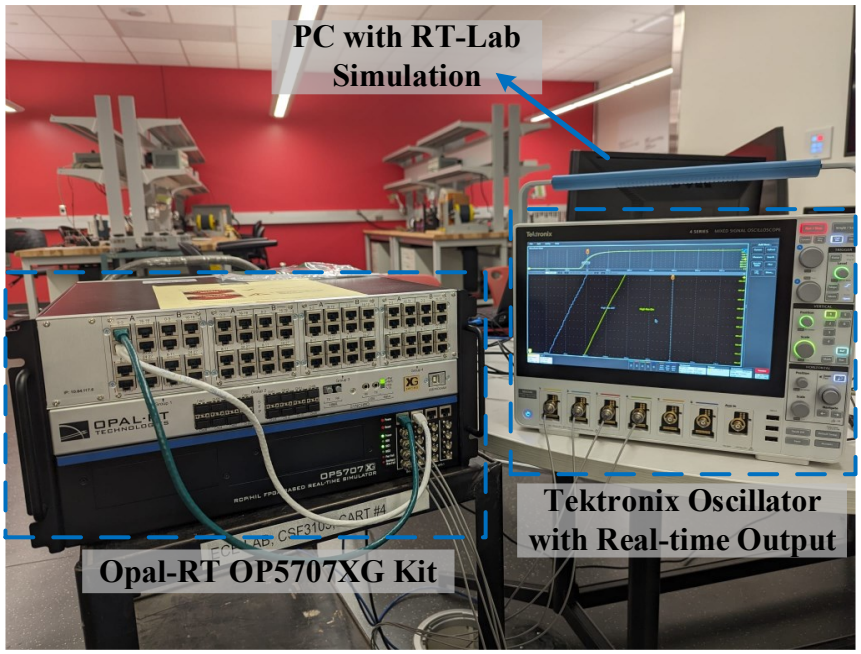

Figure 15. Opal-RT Simulator Setup

The general parameters of the circuit under simulation are provided in Table below:

Table 3. Interleaved Operation Design Parameters

Technical Specification	***Value***
Nominal Input Voltage (V)	750
Nominal Output Voltage (V)	28
Nominal Output Power (W)	5600
Output Impedance (Ω)	0.14
Switching Frequency (kHz)	50
High Voltage MOSFET Voltage (V)	1200
High Voltage MOSFET Current (A)	120
LV MOSFET Voltage (V)	80
LV MOSFET Current (A)	180
Transformer Turn Ratio (n)	30:1:1
Bridge Inductor Value (μH)	150
Output Capacitor (mF)	12
Output Capacitor ESR (mΩ)	2.2

Simulink was used to create a model of a bi-directional two-stage EV charger that is suitable for both V2G and G2V operations. Figure 12 shows the model, which consists of but not limited to many components such as a supply grid, input filters, a full bridge front-end converter, a buck-boost converter, a battery, and a simulated induction motor. Since the supply grid is specified as 415 V, the 3 level LCL filter acts as a three-phase swing bus, reducing supply harmonics and correct power factor.

The output of the filters is then given to the front-end converter (FEC) for AC to DC conversion, which uses a full bridge converter with six IGBT switches and a PWM technique for power conversion. The desired value of DC bus voltage on the output of FEC is set at 400V.

The bi-directional buck/boost converter is connected to the output of the FEC and is used to control the battery current during charging and discharging operations. MOSFETs are used to simulate the buck/boost converter and gate pulses are generated from a PI controller.

Finally, the battery used in the simulation is of Li-ion type with the initial state of charge (SOC) set to 50%. Three-phase circuit breakers are used to simulate the changeover between the battery and the grid on the AC side of the converter.

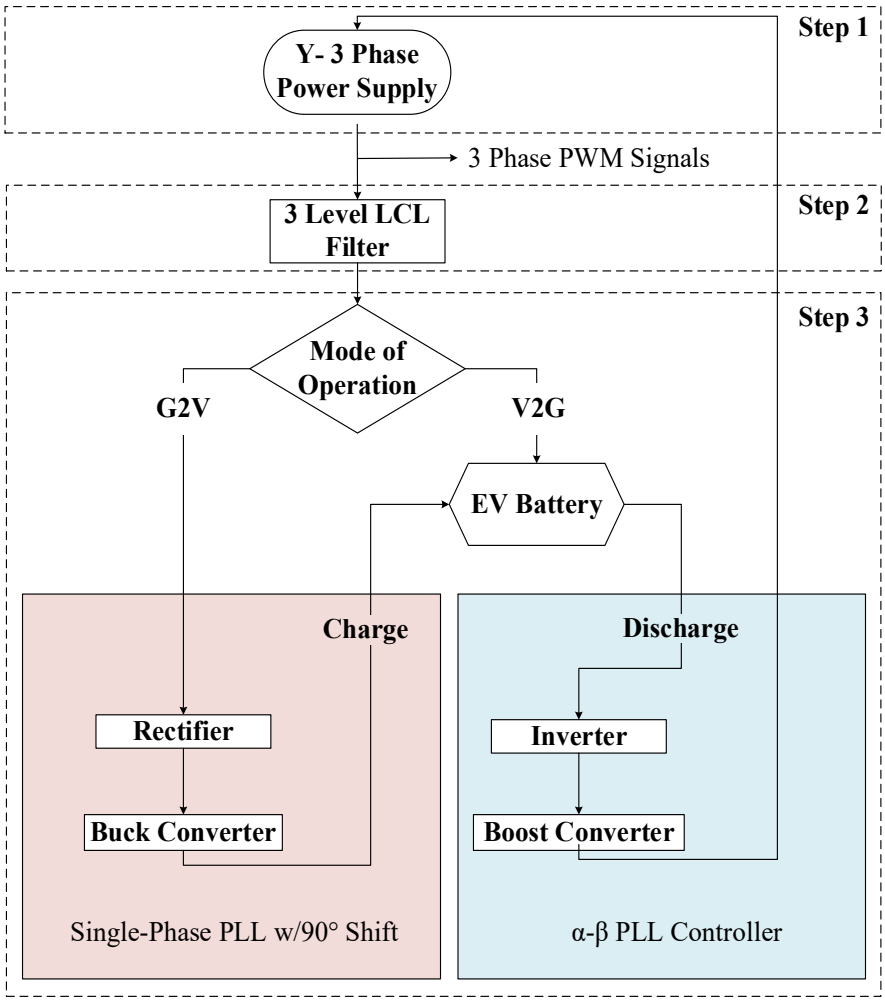

Figure 16. Flow Chart for the G2V/V2G PLL Controllers

The developed Simulink model constitutes a two-stage, bidirectional EV charger, designed for both G2V and V2G functionalities. For G2V charging, the model harnesses a 3-phase Y-connected supply, mimicking grid power, where switches serve as rectifiers. In this mode, breaker 1 is engaged while breaker 2 is disengaged, establishing a connection to the grid supply. The pulse generator for the buck/boost converter is programmed with a steady input.

Activation of the converter involves introducing AC voltage through an LCL filter, followed by its passage through switches functioning either as inverters or rectifiers, ultimately reaching the buck or boost converter.

The operational mode, either V2G or G2V, is determined by a fixed input that accordingly tailors the PWM pulse signals for the switches. The simulation yields various parameters, which are graphically depicted. Notably, in V2G mode, there exists a synchronization between voltage and current (aligning with grid synchronization requirements), a characteristic not present in G2V mode, as illustrated in Figure 17 below:

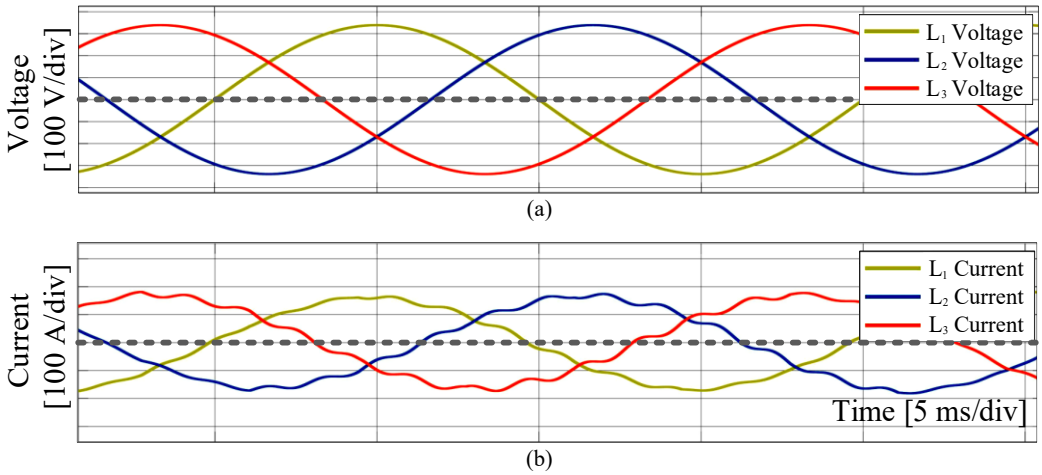

Figure 17. Simulink Output of 3-Phase G2V Voltage Signals

The amount of power to be transferred by the DAB circuit topology, neglecting harmonics, is calculated as shown in the equation:

$$P_{transferred} = \frac{V_1 V_2}{n X_L} \sin(\theta) \tag{10}$$

Here, V1 represents the effective value of the transformer primary winding voltage, V2 represents the effective value of the voltage on the output side of the energy transfer inductor, XL represents the reactance value of the energy transfer inductor at the switching frequency, n represents the transformer turn ratio, and θ represents the phase shift value on the AC side. According to Equation 10, the amount of power transferred varies depending on the amplitude of the square wave signal in both H-bridge circuits, the value of the energy inductor, and the sine of the phase difference between the AC side voltage and the DC side square wave voltage.

For a phase shift value of 36°, the driver signals for the MOSFET switches on both the AC and DC sides are shown in Figure:

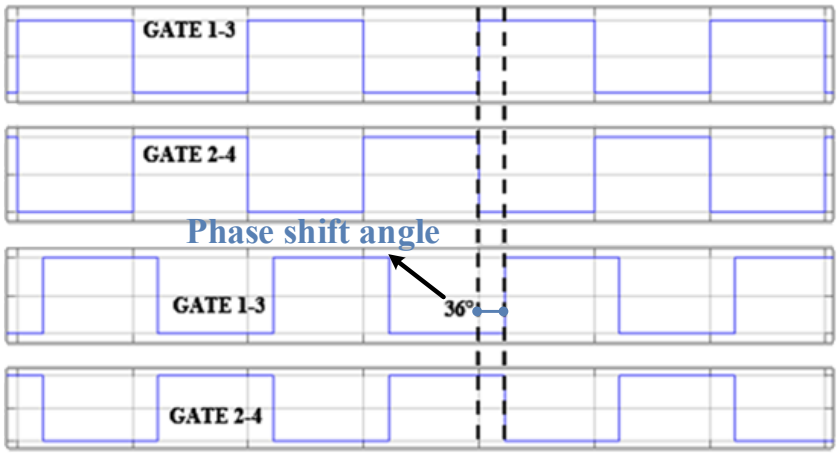

Figure 18. MOSFET Driver Signals for Low and High Voltages

Assuming the inductor value is fixed after the design phase, the parameter controlling the changing power or voltage values is the phase shift value between the two H-bridges. The phase shift value varies between 0°-360°, and after 180°, the direction of power flow changes. Figure 19 shows the voltage waveforms at the inductor input and output and the inductor current waveform after the applied phase-shifted signals:

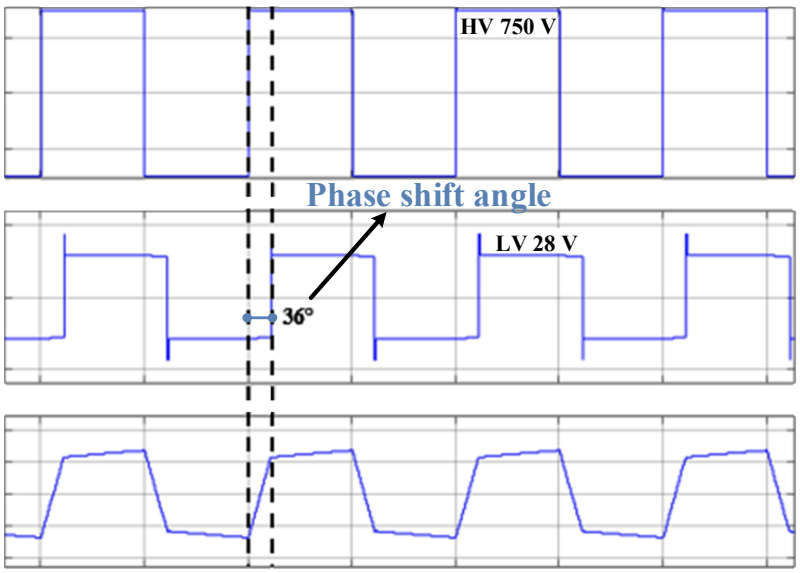

Figure 19. Inductor Input-Output Voltages with Inductor Current Waveform (Top to Bottom)

As seen from equation 5 and the figures 18 and 19, the amount of transferred power increases as the phase shift value increases.

4.2. Power Semiconductor Loss and Conduction Losses for the DC Side

Power semiconductor losses for a single 5.6 kW DAB converter unit are given in this section. Discrete package silicon carbide switches have been used for the high voltage H-bridge switches. The silicon carbide switch has a typical conduction resistance of 25 mΩ at 1200 V, 60 A voltage and current values.

When the silicon carbide switch is driven at Vgs = 20 V, according to the simulation result in Figure 20, the drain-source current Ids is approximately 8 A rms. Using the conduction resistance Rds of approximately 43 mΩ for the worst-case scenario, the MOSFET drain-source voltage is approximately Vds = 0.4 V. Therefore, the conduction loss value for each switch in the input H-bridge circuit of the converter is 3.2 W, totaling 12.8 W for the entire H-bridge. The conduction loss for each MOSFET based on the simulation result is shown in Figure 21. As can be seen, the calculated conduction loss value is approximately the same as the simulation results.

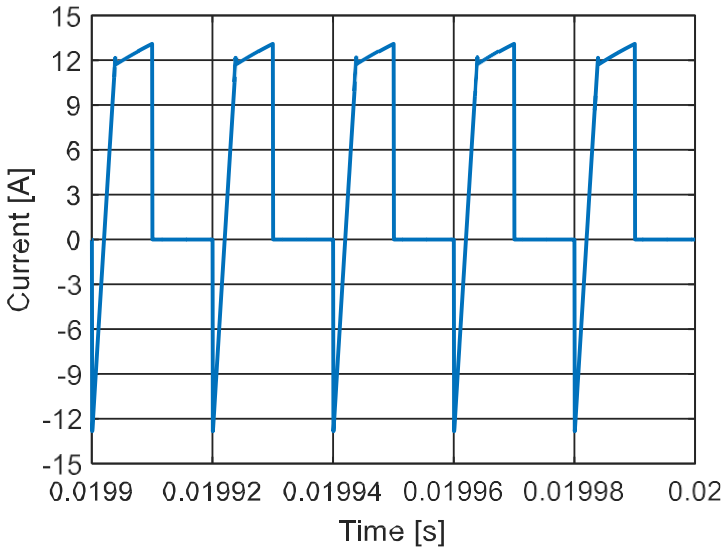

Figure 20. Simulation Result for The Drain-Source Current of the Input H-Bridge Silicon Carbide Switch.

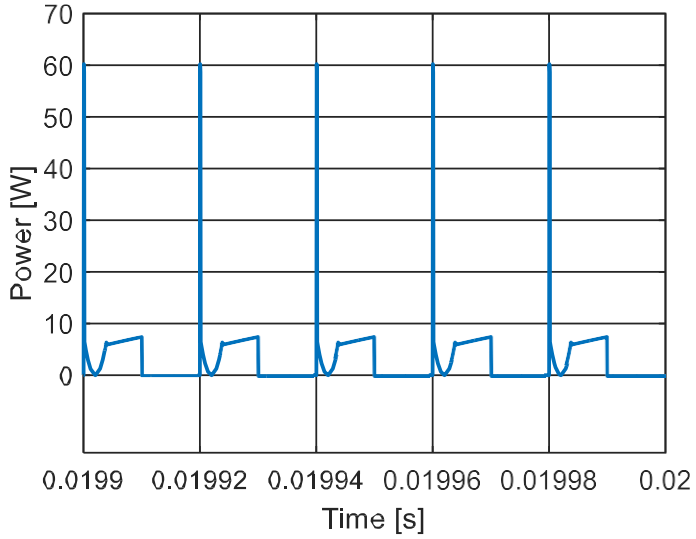

Figure 21. Simulation Result of Input H-Bridge Silicon Carbide Switch Conduction Loss

4.3. Switching Losses

With the input DC voltage of the converter H-bridge at 800 V and the silicon carbide switch drain-source current $I_{ds} \approx 8A$ rms, the total switching loss energy according to the switch datasheet is 0.3 mJ. Thus, the switching loss value for each switch in the input H-bridge circuit of the converter is 15 W, making the total H-bridge switching loss 60 W. The calculated switching losses for each switch during conduction and turn-off match the simulation results. The simulation results are shown in Figure 22 and Figure 23, respectively:

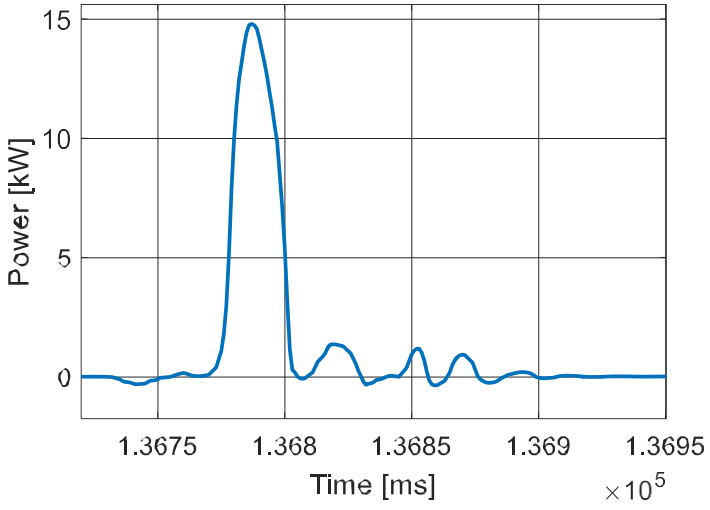

Figure 22. Switching Loss During Conduction at H-Bridge Silicon Carbide Switches

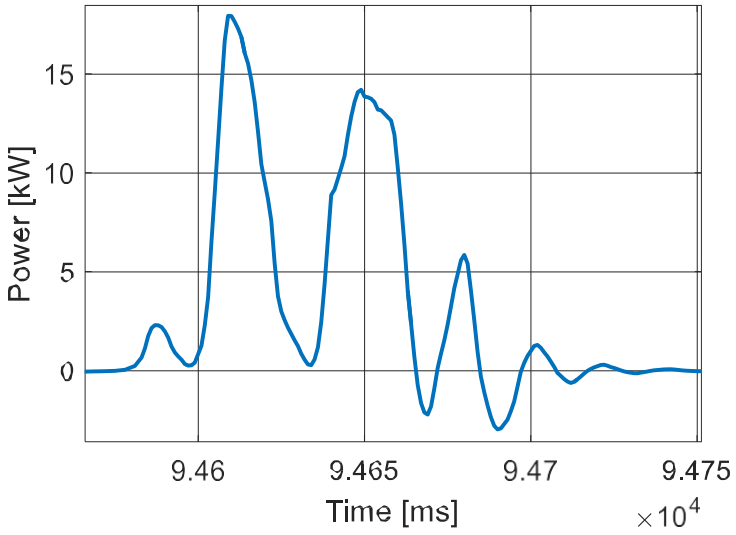

Figure 23. Switching Loss During Cut-Off at H-Bridge Silicon Carbide Switch

Consequently, the total loss for the switches on the input side of the converter is calculated as 72.8 W. Figure 22 shows the simulation result for switching loss during conduction for the input H-bridge silicon carbide switch. Figure 23 shows the simulation result for switching loss during cut-off for the input H-bridge silicon carbide switch.

4.4. Power Semiconductor and Conduction Losses Calculations for the AC Side

Discrete package silicon switches with very low on-resistance values have been used for the low-voltage H-bridge switches. Since much higher currents flow through the converter's output stage compared to the input stage, the conduction losses, and therefore the drain-source resistance, become very significant. Each switch in the output H-bridge circuit is used in a 3-parallel configuration to further reduce the on-resistance and minimize conduction losses. The easy paralleling capability of silicon MOSFET switches also provides an advantage for the application. The selected silicon switch has a typical on-resistance of 1.9 mΩ with voltage and current ratings of 80 V and 180 A, respectively.

When the silicon switch is driven at $V_{gs} = 10V$, according to the simulation result shown in Figure 24:

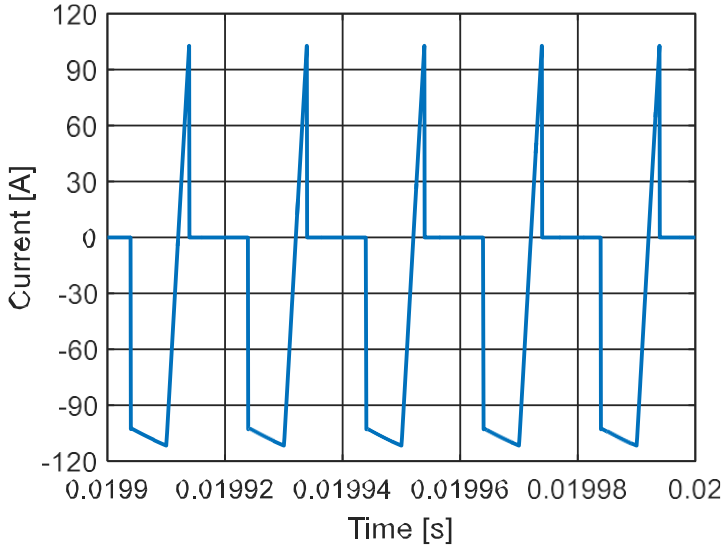

Figure 24. Simulation Result of the Drain-Source Current of the Output H-Bridge Silicon Switch

The drain-source current $I_{ds} \approx 66A$ rms. Using the on-resistance $R_{ds} \approx 1.9m\Omega$ provided in the datasheet for the worst-case scenario, the MOSFET drain-source voltage is approximately $V_{ds} \approx 0.14V$.

Therefore, the conduction loss value for each switch in the output H-bridge circuit of the converter is 9.3 W, making the total H-bridge conduction loss for all 12 switches 112 W. The simulation result for the drain-source voltage of each MOSFET is shown in Figure 25 below:

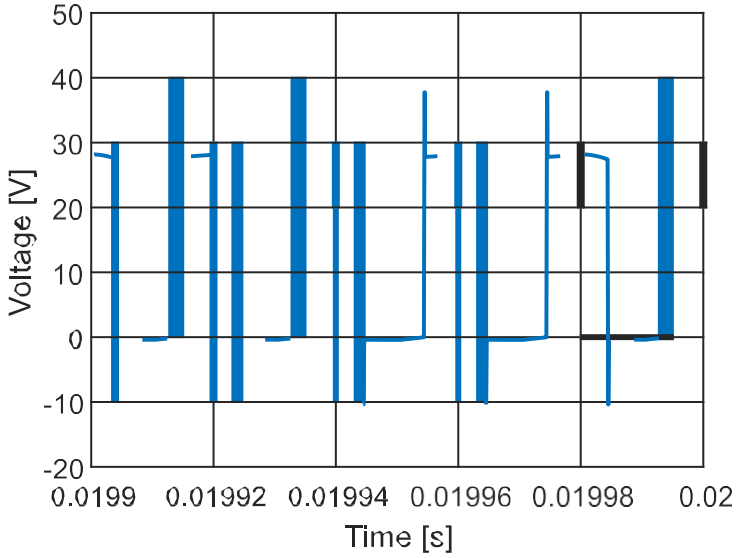

Figure 25. Simulation Result for The Drain-Source Voltage of the Output H-Bridge Silicon Switch

4.5. Switching Losses

With the output DC voltage of the converter at 28 V and the drain-source current value of each silicon switch $I_{ds} \approx 66A$ rms, the total switching loss energy according to the switch datasheet is 0.01928 mJ. Thus, the switching loss value for each switch in the output H-bridge circuit of the converter is approximately 1 W, making the total H-bridge switching loss for 12 switches 12 W. The conduction loss simulation results for each MOSFET are shown in Figures 26 and 27, respectively. According to conduction and switching losses, the total loss for silicon switches in the output stage is 124 W.

It's important to note that the conduction losses of the output silicon switches are significantly higher than those of the input silicon carbide switches. As the drain-source resistances change with temperature, the drain-source resistance should be recalculated based on the realistic operating condition temperature value provided in the switch datasheet, and the switch losses should be reassessed for this worst-case scenario.

If it is assumed for this study that the operating temperature of the output silicon MOSFET switches is 100 °C, the on-resistance would be approximately $R_{ds} \approx 2.6m\Omega$, making the total conduction loss 136 W. With the updated R_{ds}, the total power loss for the output stage switches is 148 W.

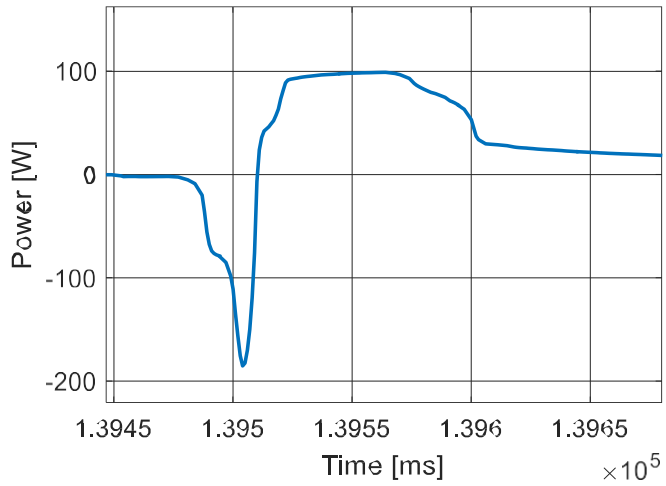

Figure 26. Simulation Result for Switching Loss During Conduction for the Output H-Bridge Silicon Switches.

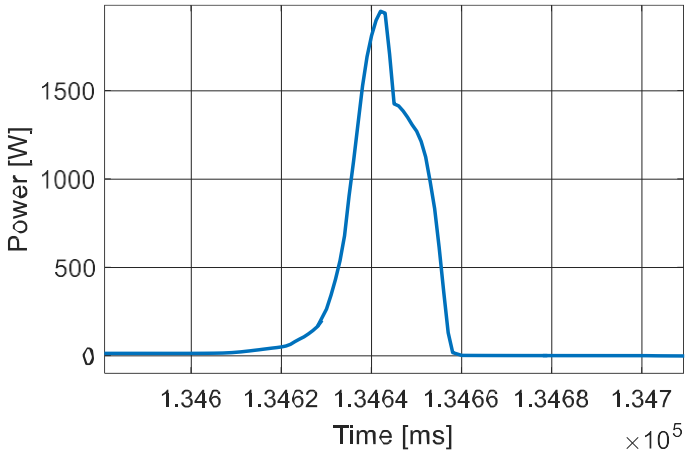

Figure 27. Simulation Result for Switching Loss During Turn-Off for the Output H-Bridge Silicon Switches.

4.6. Determining the Optimal Value of the Energy Transfer Inductor

To enable the converter to operate under various load and input voltage conditions, it is necessary to determine the optimal value of the energy transfer inductor. The converter must be able to deliver maximum current values between the minimum and nominal output voltages, and power transfer should be limited when the output voltage exceeds the nominal voltage.

As seen in Figure 8-9, the minimum output voltage is 16 V, at which the converter must deliver a total output current of 260 A. In this condition, the input voltage is 450 V. The phase angle for the converter's operating conditions will be determined at this operating condition. As understood from Equation 5, the value of the phase angle varies significantly for input voltages of 750 V and 450 V when the inductor value and power are fixed. This helps determine the limits of the phase angle.

Another important point is that to operate at the same power point, an increase in the phase shift value requires an increase in the inductor value. Additionally, increasing the inductor value leads to an increase in the output capacitor ripple currents, thus necessitating a larger capacitor value. Figure 28 illustrates the change in inductor value corresponding to the phase shift change at the same power level (11.2 kW). Figure 29 shows the change in the effective value of the output capacitor current as the inductor value increases.

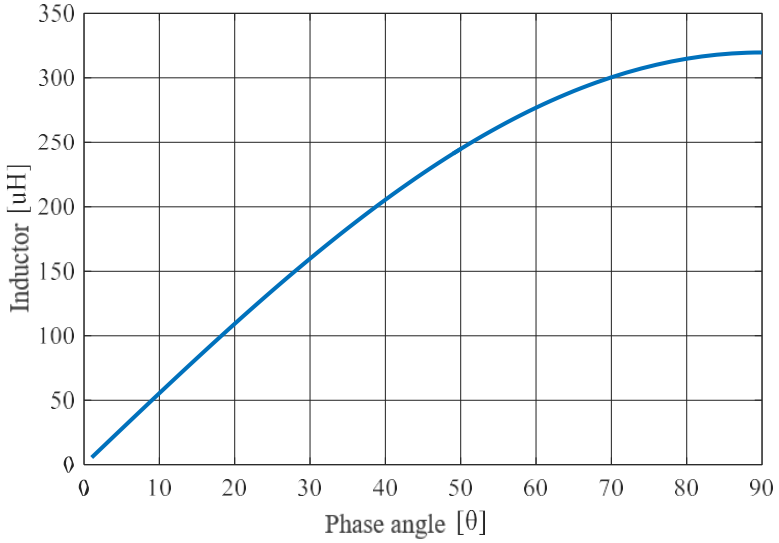

Figure 28. Change In Inductor Value According to The Phase Shift Value for The DAB Converter.

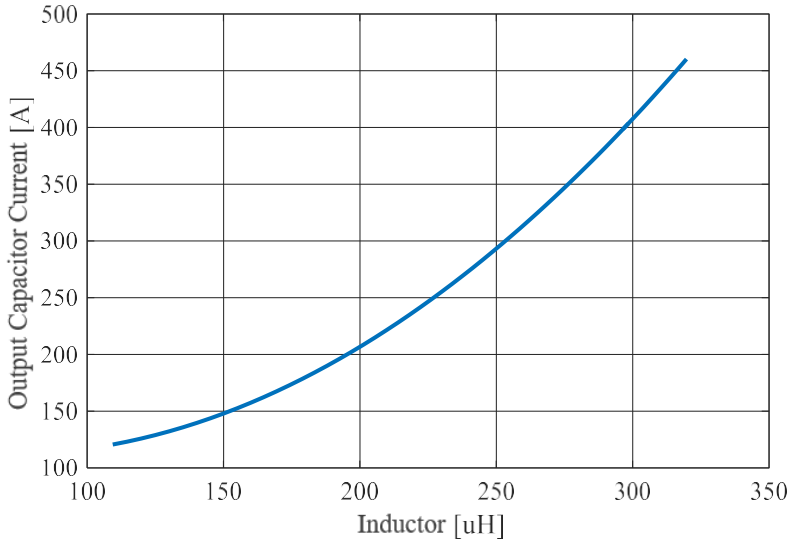

Figure 29. Change In Output Capacitor Current Due to the Change In Inductor For the DAB Converter.

When simulation studies are conducted, the inductor value to be used on the primary winding side of the transformer is 150 µH, and the phase value is around 16°. Moreover, the results obtained from simulations for different power and input voltage values are summarized in Table 4.

As seen from Table 4, for the worst-case scenario with an input voltage of 450 V, the phase shift needs to be around 85° to transfer 5.6 kW of power. Another point noted in Table 4 is the increase in output capacitor ripple current as the inductor value is raised for a power value of 11.2 kW. Reducing the inductance value too much causes the phase angle value at full power to decrease, leading to very small angle values at lower powers and affecting control precision adversely.

Table 4. Changes In Converter Parameters for Different Power, Input Voltage, and Inductance

Power (kW)	**Input Voltage (V)**	**Output Voltage (V)**	**Inductance Value (µH)**	**Phase angle (Degrees)**	**Inductor Current(A)**	**Output Current (A)**
11.2	750	28	100	23.4	117	79
11.2	750	28	150	38	148	82
11.2	750	28	220	88	238	117
5.6	750	28	150	16.2	40	38
2.8	750	28	150	7.2	28	20
5.6	450	16	150	85	196	97

The selection of capacitors in the input and output stages of the DAB converter considered the following factors:

- Ripple current carrying capacity
- ESR and ESL values,
- Maximum operating temperature value,
- Resistance to environmental conditions such as humidity and vibration,
- Availability for automotive applications,
- Size and volume,
- Weight.

Especially since there's no filter inductor on the output stage of the DAB converter, the bus capacitor is exposed to high RMS ripple currents, and choosing an appropriate capacitor value is crucial for the operation of the converter.

Upon examining Equation 5, it's evident that the factors affecting the RMS value of the output capacitor current are:

- The value of the energy transfer inductor (L)
- The phase shift value on the AC side (θ)

These two values determine the power the DAB converter will transfer to the load and, consequently, the output current and capacitor ripple current. Inserting the nominal operating values from Table 4 into Equation 5 yields the values in Table 5.

Table 5. Change in Output Capacitor RMS Current for Different Circuit Parameters

L (mH)	**θ (°)**	**I_{crms} (A)**	**Ease of Control**
0.4	72	200 A	Sensitive
0.25	36	110 A	Normal

Table 5 shows the inductance value based on the phase shift value as a reference. The maximum limit of the phase shift value for power transmission from the DC to the AC side is 90°. At this value, the output power is maximized and then decreases again up to 180°. Beyond this value, the direction of power flow changes. To avoid approaching the limit value too closely and because the capacitor ripple current increases as it approaches the limit values, the phase shift starting value is chosen as 72°. Selecting a higher phase shift allows for more precise control of the output voltage over a wider range.

Figures 30, 31, 32, and 33 show the output capacitor voltage waveform and effective current value for phase shift values of 36° and 72°, respectively.

When the phase shift value is halved, and the inductance value is calculated from Equation 5, the output capacitor ripple current is seen to be nearly halved. This result is considered more reasonable in terms of converter sizes and capacitor temperature values. When examining commercial products, it is observed that the output voltage ripple value has a wider range, hence lower capacitor values are used.

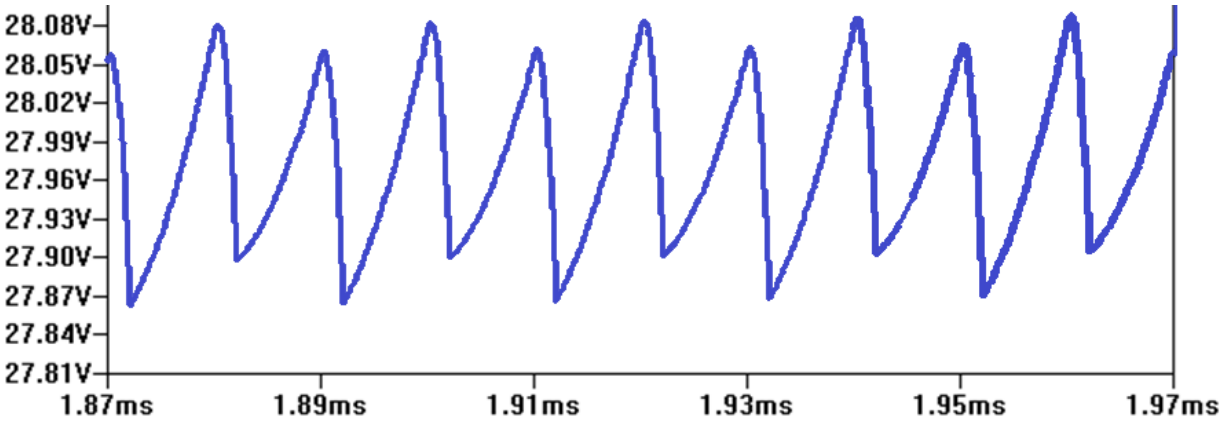

Figure 30. Converter Output Voltage Waveform for a Phase Shift Angle Of 36°

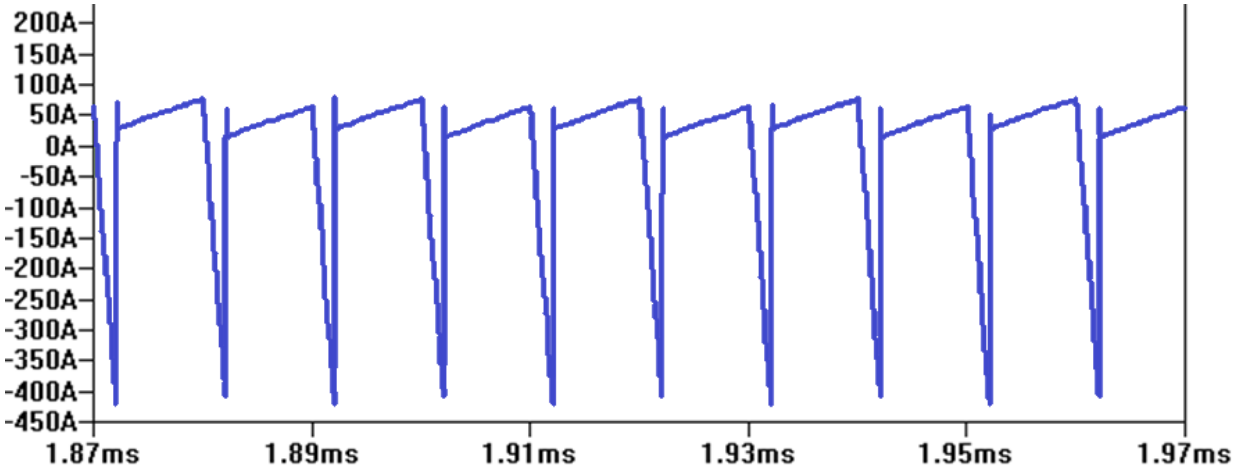

Figure 31. Converter Output Current Waveform for a Phase Shift Angle Of 36°

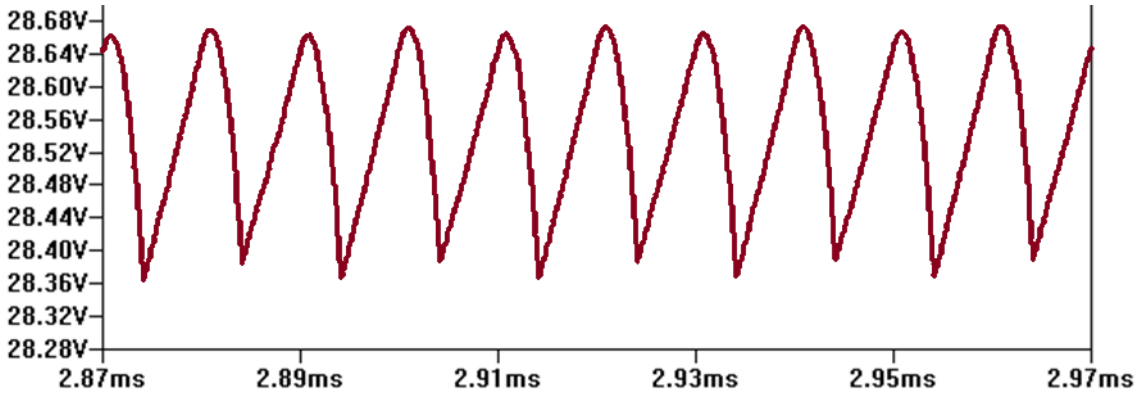

Figure 32. Converter Output Voltage Waveform for a Phase Shift Angle Of 72°

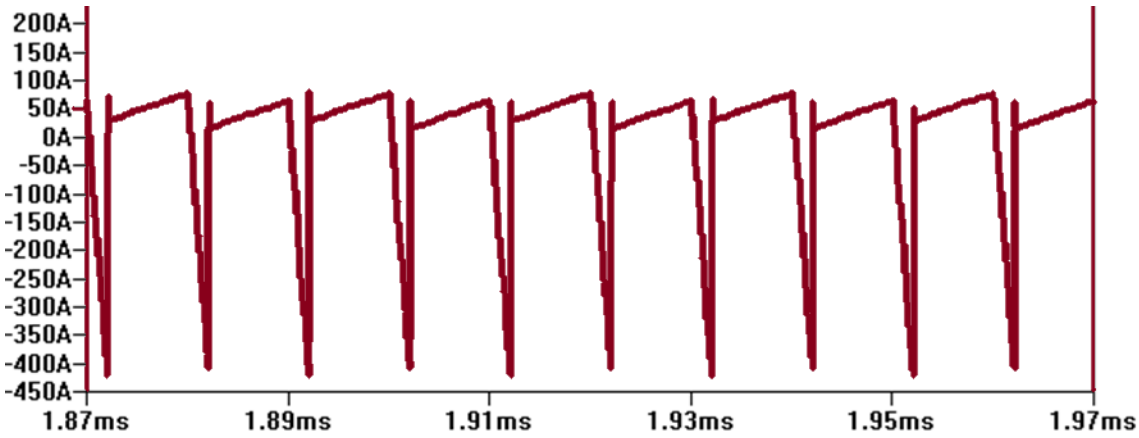

Figure 33. Converter Output Current Waveform for a Phase Shift Angle Of 72°

Simulations for nominal operating conditions were conducted with an output capacitance value of 3mF and an ESR value of 3 mΩ. For both phase shift angles, the converter output voltage ripple value (peak-to-peak) is smaller than the targeted 280 mV (1% of the nominal output voltage). The effective value of the output capacitor current is 110 A for a phase shift angle of 36° and 200 A for a phase shift angle of 72°. According to these results, an electrolytic or metal film type capacitor with a capacity value of 3 mF, an equivalent series resistance of 3 mΩ or lower, and a 100 A rms current carrying capability is required for the DAB converter output capacitor. Commercial products for metal film capacitors at these capacity values are very limited and occupy a lot of volume when used in parallel. Therefore, electrolytic type capacitors, which have higher energy densities and relatively smaller sizes, are preferred in this study.

The selected capacitor is of the aluminum electrolytic type, designed for automotive applications, capable of operating up to 150°C, and resistant to vibrations. It has a high ripple (ripple current) carrying capacity and low ESR values. In the simulation studies, the energy transfer inductor was initially used on the secondary side of the transformer and later moved to the primary side. Calculations for capacitor selection assumed an operating temperature of 105°C. In this study, aluminum electrolytic capacitors with a capacity value of 7.2 mF, an equivalent series resistance of 2.2 mΩ, and a 147 A rms current carrying capability were selected.

4.7. Transformer Design and Losses

The technical specifications of the 20 kVA high-frequency transformer to be designed for the main 20 kW DAB converter are provided in Table 3. Based on Simulink results and to achieve the best efficiency conditions, a switching frequency of 20 kHz has been deemed appropriate. The turn ratio has been selected to transfer the rated power at the nominal input voltage level (V = 415 V AC). At a 20 kHz operating frequency, the skin depth in copper is approximately 0.30 mm. The core material has been targeted for selection from commercially available nanocrystal and ferrite core materials suitable for these power and frequency values.

A roughly square wave voltage waveform is formed at the output of the H-bridge converter. For each switch operating at a duty cycle of D = 1/2, the waveform becomes a complete square wave. The voltage waveform formed in the DC link in the DAB converter structure covered by this research close to a square wave. Using the Area Product method, the expression of the apparent power at the high-frequency input of the converter in terms of transformer design parameters is found with the help of the following equations:

$$V_{pri} = N_p \frac{d\phi}{dt} \quad (11)$$

$$V_{pri} \frac{T_s}{2} = N_p (2B_{ac} p) A_{core} \quad (12)$$

Where, for D = 1/2 and B_{ac} being the peak magnetic flux density:

$$V_{pri} = 4 f N_p B_{ac} A_{core} \quad (13)$$

$$S = V_{pri} I_{pri} = 2 k_{cu} f A_{core} A_w J_{rms} B_{acp} \quad (14)$$

Here, k_{cu} is the copper fill factor, A_{core} is the core cross-sectional area, A_w is the winding area, J_{rms} is the RMS current density, and B_{acp} is the peak value of the alternating magnetic flux density. The product of A_{core} and A_w, known as the Area Product, is a crucial parameter for the transformer to be designed. In the design, nanocrystalline core material, known for its low core losses and high saturation flux density values, has been used.

Accordingly, initial design values have been set as $k_{cu} \approx 0.4$, $J_{rms} = 3 A/mm^2$, $f = 20\ kHz$, and $B_{ac} = 0.15T$. According to Equation 14, when calculating the Area Product, $(AP = 11.72 cm^2)$. For an SU30A type nanocrystalline core, the Area Product value is 30 cm^2, which is suitable for the calculated Area Product value.

For transformer core losses, the loss values provided in any manufacturer technical documentation were used. Accordingly, for a switching frequency of 20 kHz and a value of 0.15 T, the value ratio for the graph is approximately 4 W/kg. Based on the core weight, the core loss $P_{core} \approx 2.5W$.

It's important to note that the values in the manufacturer's loss graph are for sinusoidal components, and it should be clarified whether the provided loss values are for processed core losses. Cores that have not undergone any thermal or chemical treatment tend to have lower losses compared to cores available to end consumers. Therefore, practical core losses and hence the core temperature can turn out to be higher than the calculated value. To mitigate this, choosing core types with the same Area Product values but with more surface area exposed to air can yield better thermal results.

For transformer winding losses, the resistances for both DC and AC for the windings are calculated individually and then multiplied by the relevant current values. For the highest current condition, which is 360 A DC current at the 20 kW converter output, the required conductor cross-sectional area for a current density of 3A/mm² is 42.8 mm². Due to the high frequency current and high cross-sectional value, the most suitable conductor type for the transformer secondary winding would be copper foil. To meet this cross-sectional value, 2 parallel layers of copper foil with dimensions of 43 mm x 0.6 mm are sufficient. For the primary winding, the current value is relatively low, and a conductor with a cross-section of 3 mm² is sufficient for 9 A rms current. Due to the high AC current components, Litz wire should be used in the primary winding.

Therefore, for the primary winding at 20 kHz, the skin depth ($\delta = 0.30$)mm, and if an appropriate wire cross-section is not used, the AC losses associated with the winding will be significant. For ($\delta = 0.30$) mm, the cross-sectional area of each round copper conductor should be < 0.1 mm². For a 3 mm² conductor cross-section, 26 turns winding, and a conductor length of 245 mm, the DC resistance of the primary winding ($R_{dc} = 2.3 \times 10^{-6} \times 245/0.03 \cong 19m\Omega$).

Using the Dowell ratio for the AC resistance, the resistance factor is seen to be approximately 1.5 times. The total copper loss for the primary winding for DC and AC resistances ($P_{cu} = 19 \times 10^{-3} \times 9^2 \times 2.5 = 3.8W$).

For the secondary winding with a copper cross-sectional area ($A_{cu,sec} \approx 50mm^2$), 2 parallel layers, and a conductor length of 100 mm, ($R_{dc} = 2.3 \times 10^{-6} \times 10/0.25 = 0.089m\Omega$). The resistance factor is approximately 1. Hence, the total winding loss for the secondary winding ($P_{cu} = 2 \times 0.089 \times 10^{-3} \times 130^2 \times 2 = 5.8W$). Therefore, the total copper loss is 9.6 W, and the total transformer loss is approximately 25 W.

For the calculation of temperature rise, the thermal resistance of the core, calculated based on the core winding area using the equation ($R_{th} = 36/A_w$) in cm^2, has been utilized. For $A_w = 9cm^2$, the core thermal resistance is approximately calculated as $4\ °C/W$. Therefore, for a total transformer loss of 25 W, the temperature rise ($\Delta T = R_{th}P_{total} = 4 \times 25 = 100°C$), leading to a final transformer temperature of $T = 25 + 100 = 125\ °C$ for an ambient temperature of 25°C. Considering the selected core and winding temperatures have a maximum operating temperature of 150°C, this value is appropriate.

Similar to the high-frequency transformer design, the high-frequency inductor design has been conducted using the Area Product method, initially calculating the inductor Area Product with the help of Equation 14. Unlike the transformer, where the instantaneous transferred power value is considered, the design here is based on the energy stored by the inductor. Therefore, the expression on the left side of the equation represents the energy stored by the inductor ($LI_pI_{rms} = 2k_{cu}fA_{core}A_wJ_{rms}B_{ac}p$). The equation provided reflects the approach of calculating the energy stored by the inductor based on the inductor's inductance value L, the peak current I_p, the RMS current I_{rms}, the copper fill factor k_{cu}, the core cross-sectional area A_{core}, the winding area A_w, the RMS current density J_{rms}, and the peak magnetic flux density B_{acp}.

In the design, a predetermined inductance value of 20 mH, a peak current I_p of 12.5 A, and an RMS current I_{rms} of 9 A were used. The initial design values were set as $(k_{cu} \approx 0.3), (J_{rms} = 3.8A/mm^2), and (B_{ac} = 0.15T)$. Based on these values, the Area Product (AP) was calculated to be $(AP = 150 \times 10^{-6} \times 110/(0.3 \times 3.8 \times 10^6 \times 0.15) = 8.5cm^2)$. For an SU38A type nanocrystalline core, the Area Product value is approximately 12 cm^4, which is suitable for the calculated Area Product value.

For the inductor core losses, a switching frequency of 20 kHz and a magnetic flux density of 0.15 T, the value from manufacturers is approximately 6 W/kg. Based on the core weight, the core loss $(P_{core} \approx 2W)$.

5. Experimental Results

The experimental results of the designed 50 kHz converter are presented under this heading. The first section provides a visual of the converter, while the subsequent section shares the experimental results showing the converter's performance and presents the efficiency graph under different load conditions.

The power stage and general unit view of the designed converter are shown in Figure 34. Basically, it consists of a single-phase H-bridge circuit based on silicon carbide switches at the input stage, a high-frequency inductor, a high-frequency transformer, an output rectifier circuit with silicon switches, and aluminum electrolytic type output capacitors, along with a breadboard to contain the programmable PIC18F67K22 microcontroller.

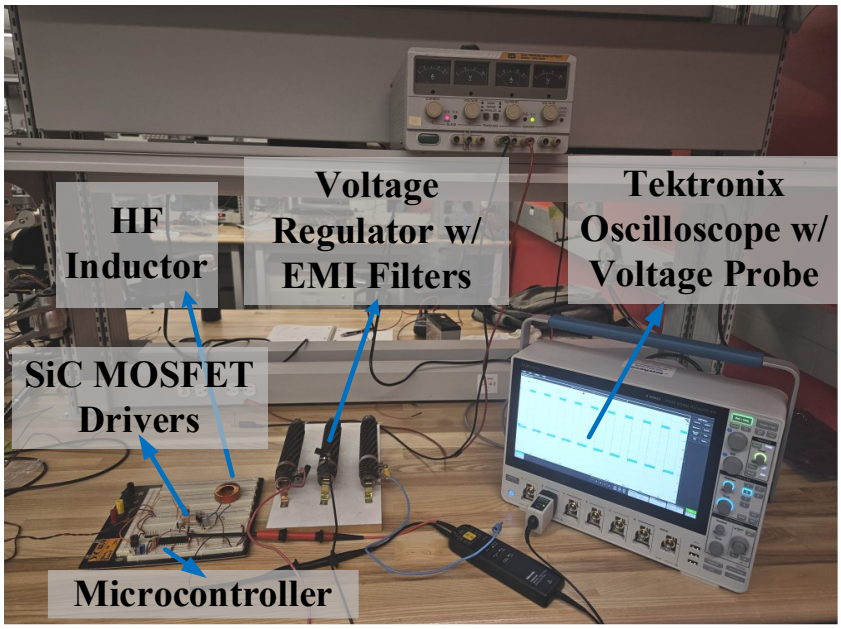

Figure 34. Lab Model of a 5.6 kW DC-AC Converter

The performance of the developed DAB converter was tested in a laboratory environment to verify soft switching, soft-start, equal current sharing control, thermal stability, and the overall efficiency of the system.

5.1. Soft Start Analysis

The experimental results obtained are presented under this heading. Firstly, the converter output voltage and the current waveforms of the energy transfer inductor for the soft-start control applied to the 14 V vehicle battery of a light electric vehicle are shown in Figure 35:

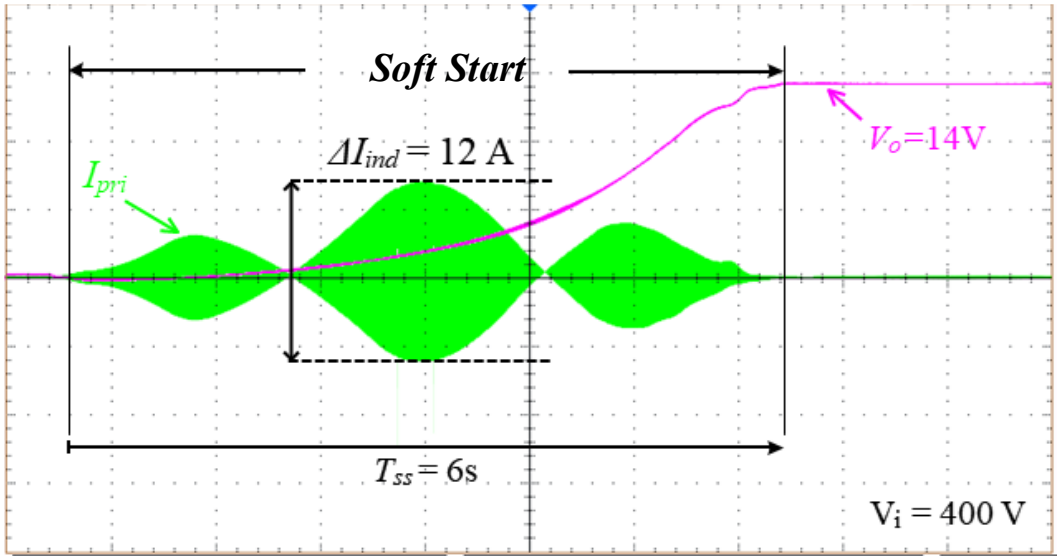

Figure 35. Primary Current of the Transformer and Converter Output Voltage During Soft Start

The purpose of the soft-start control is to prevent the capacitors with high energy capacity on the output board from drawing sudden high currents when the nominal voltage is applied to the converter input, thereby protecting the circuit components from potential disruptive effects. Since there is no filter inductor at the output of the DAB converter, high capacitance values are used to keep the output voltage ripple below a certain level. Therefore, a soft-start technique is necessary to prevent these capacitors from drawing high inrush currents initially. The soft-start technique in this study is implemented by phase shifting within the H-bridge switches on the primary side.

During the soft-start, the MOSFET switches on the secondary side are in the cutoff state, and only the body diodes are conducting, making it function like a full-bridge rectifier circuit.

A proportional-integral control technique is used for soft-start control, preventing the input current from reaching high values until the output capacitors reach the appropriate voltage level. As seen in Figure 35, the peak-to-peak current value through the inductor during the soft-start is 12 A. Several different current waveforms in Figure 35 result from the power flat region where no increase in output power is observed despite the increase in phase shift between the bridges, as previously mentioned. It takes approximately 6 seconds for the output voltage to reach the set value of 14 V. This duration can be shortened with higher inrush currents by changing the values of the proportional-integral controller.

The waveforms of the primary and secondary voltages of the transformer and the inductor currents at half load are shown in Figure 36; At this moment, the DC currents in each parallel H-bridge on the secondary side and the output voltage are also shown in Figure 37:

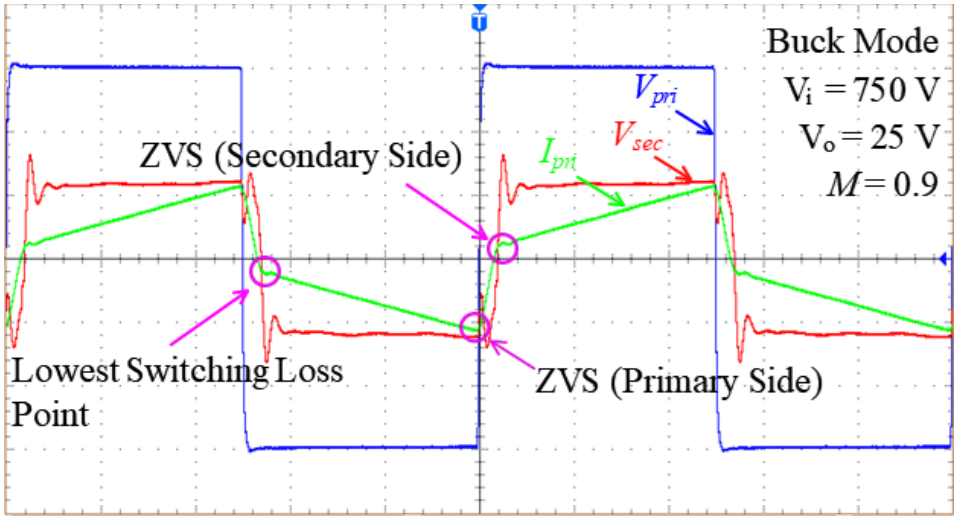

Figure 36. Transformer Primary Voltage, Current, and Inductor Current Waveform

5.2. Voltage Switching Analysis

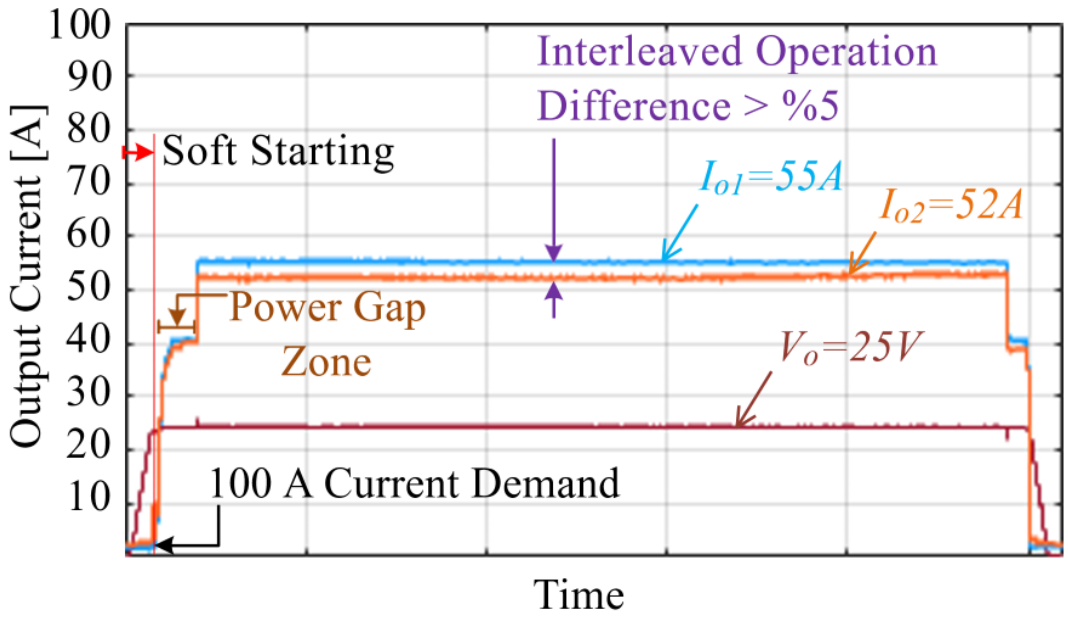

Figure 37. AC Currents for the Secondary Side H-Bridges

As seen from the inductor current waveform in Figure 37, the converter is operating in buck mode, and due to the current being positive in the regions marked in green, both the primary and secondary side switches are performing zero voltage switching. Since the inductor current is symmetrical for one switching cycle, the switches on the secondary side operate with minimal switching losses. The voltage gain of the DAB converter in Figure 37 is approximately M = 0.9. When the voltage gain of the DAB converter is one or greater, the MOSFET switches on the secondary side of the converter experience high switching losses during cutoff periods. Therefore, the value of the converter's voltage gain is of great importance both in terms of losses and efficiency under normal operating conditions. On the other hand, when the voltage gain of the converter is less than one, the MOSFET switches on the primary side are exposed to high switching losses.

However, due to the lower current values on the primary side and the low switching losses of the silicon carbide switches, this disadvantage is much lower compared to the Si MOSFET switches on the secondary side.

The current sharing graph between the parallel H-bridges on the secondary side of the converter is shown in Figure 37. As can be seen, the current sharing between the H-bridges is very close to ideal conditions. The current sharing difference between the H-bridges is less than 5% for half load. Equal current sharing is designed to control the DC current in each parallel branch with a proportional-integral controller to reduce the current difference to zero. To prevent excessive current from flowing through a single branch, the converter is shut down as a safety measure if the current sharing exceeds 10%.

Figure 37 also shows the soft-start region and the power flat region. As can be seen, in the power flat region, despite the increase in phase shift value, the output current remained the same up to a certain level and then increased to the desired value.
The same voltage waveforms were taken for the boost mode under half-load conditions and are shown in Figure 38. As seen in the figure, although the inductor current is positive, zero-voltage switching could not be achieved due to the voltage gain being greater than one.

The hard switching waveform resulting from the primary side switches not fully discharging their output capacitors is clearly visible in Figure 38. On the other hand, due to the boost operating mode, the switches on the secondary side also experience high switching losses during cutoff.

Based on the waveforms in Figures 37 and 38, the battery voltage, current, and state of charge characteristics should be calculated for the most suitable converter design and efficiency:

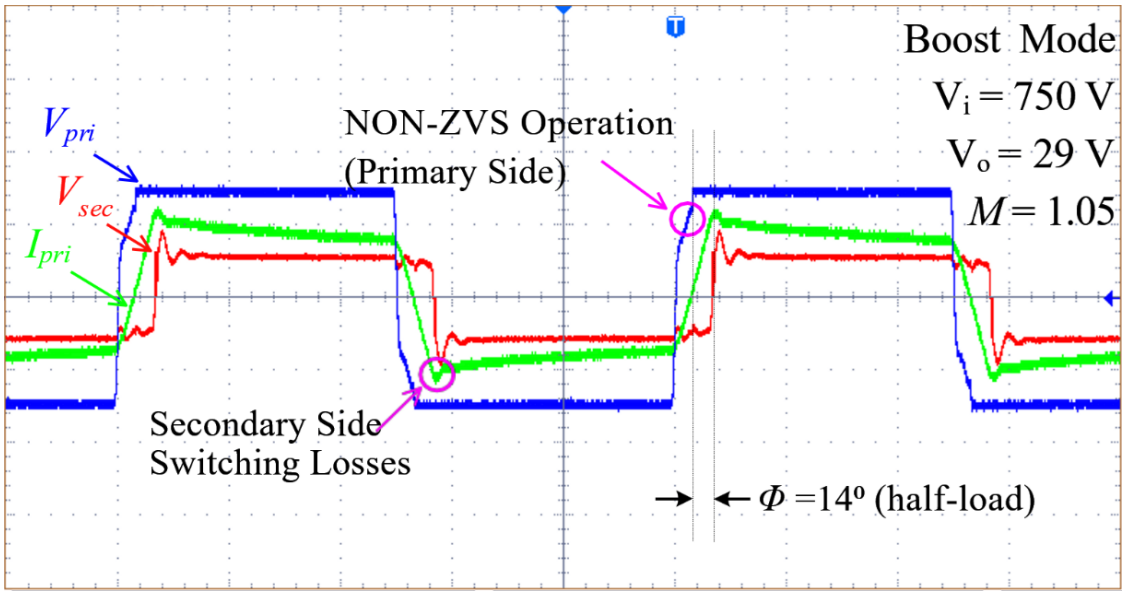

Figure 38. Waveforms of the Converter Operation for Boost Mode

The efficiency of the DAB converter, both theoretically calculated and experimentally measured, is plotted against the output power as shown in Figure 39. The test conditions applied for the efficiency values are also provided on the same graph. As seen from the efficiency graph, the converter achieves its maximum efficiency at approximately half-load conditions, measured at 98%.

From half-load conditions onwards, the switching losses of the output power MOSFET switches become significant. For full-load conditions, the converter's efficiency is measured at 97%.

5.3. Efficiency Evaluation

The efficiency of the DAB converter, both theoretically calculated and experimentally measured, is plotted against the output power as shown in Figure 39. The test conditions applied for the efficiency values are also provided on the same graph. As seen from the efficiency graph, the converter achieves its maximum efficiency at approximately half-load conditions, measured at 98%. From half-load conditions onwards, the switching losses of the output power MOSFET switches become significant. For full-load conditions, the converter's efficiency is measured at 97%.

The overall efficiency of the converter is measured at 90% for conditions under a 10% load. Conduction losses of the switches are significant up to half-load, the switching losses of the switches become significant for efficiency values between half-load and full-load conditions.

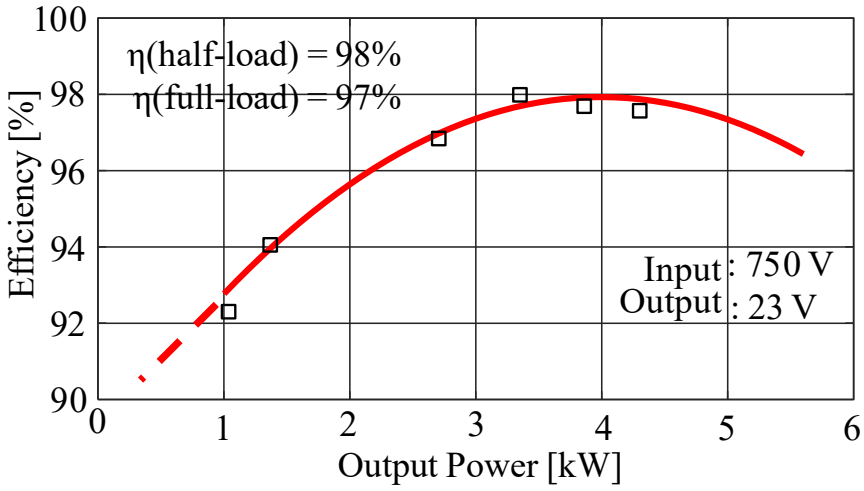

Figure 39. Efficiency Values Measured and Calculated Corresponding to the Output Power of the DC-AC Converter

6. Conclusion

In our study, a generalized DAB topology-based converter was designed and implemented for either a 750-28 V, 2 x 5.6 kW heavy electric vehicle or a 400-14 V, 3.7 kW low voltage battery charging for a light electric vehicle. Silicon carbide power MOSFET switches were used on the high-voltage H-bridge side of the converter, while silicon CoolMOS-based power MOSFET switches were used on the low-voltage side. By operating two DAB converters alternately, power levels of up to 2 x 5.6 kW can be achieved. With appropriate switching and design parameters, the high-voltage H-bridge switches perform zero-voltage switching, while the low-voltage H-bridge switches perform zero-current switching.

For the case where the DAB converter is used for a heavy electric vehicle, different load characteristics result in different operating conditions. For example, in a typical heavy electric vehicle, the power drawn from the high-voltage battery under normal operating conditions is approximately 1.4 kW. This 1.4 kW power is consumed for general needs such as the air conditioning, lighting, and dashboard power of the electric vehicle under normal operating conditions. As mentioned, the converter delivers approximately 1.4 kW of power by supplying 50 A current to the 28 V battery under normal operating conditions.

Due to the high currents that the converter output switches are subjected to, the voltage gain of the converter in its current operating condition plays a very important role in losses and, consequently, in efficiency. As seen in Figure 39, the selection of appropriate power semiconductor MOSFET switches for both the high-voltage and low-voltage sides of the DAB converter, the selection of materials, conductors, and proper winding techniques to minimize magnetic circuit element losses.

The appropriate control method results in a converter design that is both galvanically isolated and capable of operating at relatively high efficiencies. With these efficiency values, the current DAB converter design is competitive in terms of both literature and commercial products.

For the applied DAB converter, an efficiency of 97% under full-load conditions and 98% under half-load conditions was achieved at a switching frequency of 50 kHz. The use of a microcontroller for the converter power stage design, the planar design of the high-frequency transformer, and the design of the high-frequency inductor ensured the high efficiency of the DAB converter.

6.1. List of Publications

- Muhammetoglu, B.; Jamil, M. Dual Active Bridge Converter with Interleaved and Parallel Operation for Electric Vehicle Charging. Energies 2024, 17, 4258. https://doi.org/10.3390/en17174258 , Published

- “Two-Stage Variable Voltage AC-DC Converter with High-Frequency DC-Link Isolation for Vehicle to Grid (V2G) Applications”, e-Prime - Advances in Electrical Engineering, Electronics and Energy, Accepted w/ minor revision, under review

- B. Muhammetoglu and M. Jamil, "Design and Optimization of a Scalable Bidirectional DC-DC Converter for Electric Vehicle Charging Applications using SiC Switches," 2024 12th International Conference on Smart Grid, Setubal, Portugal, 2024, pp. 423-428, doi:10.1109/icSmartGrid61824.2024.10578205, Published

- “Optimizing Grid Stability and Peak Demand Reduction through Vehicle-to-Grid Services: Energy Lend-Lease Approach”, IEEE NECEC 2023, St. John’s, NL, Canada, Published

6.2. Improvements and Future Work

- Thermal Management: While the study successfully mitigates conduction and switching losses, thermal management remains a critical area for improvement. Future work could explore advanced cooling solutions or heat sink designs to further enhance efficiency and extend the converter's lifespan:

- Integration of GaN Semiconductors: The promising characteristics of Gallium Nitride (GaN) semiconductors, including higher efficiency and faster switching capabilities than SiC, could be explored in future iterations of the converter design. This could potentially lead to further reductions in size and losses.

- Advanced Control Strategies: Implementing more advanced control algorithms, such as adaptive phase shift control, could dynamically optimize the converter's performance across a wider range of operating conditions, improving efficiency and power density.

- Modular Design for Scalability: Developing a modular converter design could facilitate scalability and customization for various EV charging applications, ranging from residential to commercial and fast-charging stations.

- Integration with Renewable Energy Sources: Future studies could explore the integration of DAB converters with renewable energy sources, enhancing the sustainability of EV charging infrastructure. This includes optimizing the converter for variable input sources such as solar or wind power.

7. References

[1] C. Li et al., "Design and Implementation of a Bidirectional Isolated Cuk Converter for Low-Voltage and High-Current Automotive DC Source Applications," in IEEE Transactions on Vehicular Technology, vol. 63, no. 6, pp. 2567-2577, July 2014, doi: 10.1109/TVT.2013.2294599.

[2] W. Chen and X. Ruan, "Zero-Voltage-Switching PWM Hybrid Full-Bridge Three-Level Converter With Secondary-Voltage Clamping Scheme," in IEEE Transactions on Industrial Electronics, vol. 55, no. 2, pp. 644-654, Feb. 2008, doi: 10.1109/TIE.2007.907676.

[3] M. Jamil, B. Hussain, M. Abu-Sara, R. J. Boltryk and S. M. Sharkh, "Microgrid power electronic converters: State of the art and future challenges," in 2009 44th International Universities Power Engineering Conference (UPEC), Glasgow, UK, 2009, pp. 1-5.

[4] A. Rasool, X. Yan, U. Rasool, F. Abbas, M. Numan, H. Rasool and M. Jamil, "Enhanced Control Strategies of VSG for EV Charging Station under a Low Inertia Microgrid", in IET Power Electronics vol. 13, pp. 2895-2904. 2020, doi: 10.1049/iet-pel.2019.1592

[5] M. Andalibi, S. S. Madani, C. Ziebert, F. Naseri and M. Hajihosseini, "A Model-Based Approach for Voltage and State-of-Charge Estimation of Lithium-ion Batteries," 2022 IEEE Sustainable Power and Energy Conference (iSPEC), Perth, Australia, 2022, pp. 1-5, doi: 10.1109/iSPEC54162.2022.10032998.

[6] M. Madhukumar, T. Suresh and M. Jamil, "Investigation of Photovoltaic Grid System under Non-Uniform Irradiance Conditions," in Electronics 9, 2020, doi: 10.3390/electronics9091512

[7] A. Sufyan, M. Jamil, S. Ghafoor, Q. Awais, H.A. Ahmad, A.A. Khan and H. Abouobaida, "A Robust Nonlinear Sliding Mode Controller for a Three-Phase Grid-Connected Inverter with an LCL Filter," in Energies, 2022, doi: 10.3390/en15249428

[8] H.A. Muqeet, R. Liaqat, M. Jamil and A.A. Khan, "A State-of-the-Art Review of Smart Energy Systems and Their Management in a Smart Grid Environment," in Energies, 2023, doi: 10.3390/en16010472

[9] D. Das, N. Weise, K. Basu, R. Baranwal and N. Mohan, "A Bidirectional Soft-Switched DAB-Based Single-Stage Three-Phase AC–DC Converter for V2G Application," in IEEE Transactions on Transportation Electrification, vol. 5, no. 1, pp. 186-199, March 2019, doi: 10.1109/TTE.2018.2886455.

[10] Z. Fang, H. Yue, F. Xie and Z. Huang, "Non-Backflow-Power and Reduced-Switching-Loss Modulation for Bidirectional Series Resonant Converter With Wide Gain Range," in IEEE Journal of Emerging and Selected Topics in Power Electronics, vol. 11, no. 1, pp. 490-505, Feb. 2023, doi: 10.1109/JESTPE.2022.3207002.

[11] Z. Wang, Y. Zhang, S. You, H. Xiao and M. Cheng, "An Integrated Power Conversion System for Electric Traction and V2G Operation in Electric Vehicles With a Small Film Capacitor," in IEEE Transactions on Power Electronics, vol. 35, no. 5, pp. 5066-5077, May 2020, doi: 10.1109/TPEL.2019.2944276.

[12] X. Zhan, H. Wu, Y. Xing, H. Ge and X. Xiao, "A high step-up bidirectional isolated dual-active-bridge converter with three-level voltage-doubler rectifier for energy storage applications," 2016 IEEE Applied Power Electronics Conference and Exposition (APEC), Long Beach, CA, USA, 2016, pp. 1424-1429, doi: 10.1109/APEC.2016.7468055.

[13] Y. Li, Y. Wang, Y. Guan and D. Xu, "Optimized Bidirectional DC-DC Converter Adapted to High Voltage Gain and Wide ZVS Range," in IEEE Transactions on Power Electronics, vol. 38, no. 3, pp. 3486-3499, March 2023, doi: 10.1109/TPEL.2022.3221946.

[14] S. Gopinathan, V. S. Rao and K. Sundaramoorthy, "Family of Non-Isolated Quadratic High Gain DC–DC Converters Based on Extended Capacitor-Diode Network for Renewable Energy Source Integration," in IEEE Journal of Emerging and Selected Topics in Power Electronics, vol. 10, no. 5, pp. 6218-6230, Oct. 2022, doi: 10.1109/JESTPE.2022.3167283.

[15] M. Aalami, E. Babaei and S. Ghassem Zadeh, "Coupled Inductor Assisted High-Voltage Gain Half-Bridge Z-Source Inverter," in IEEE Open Journal of the Industrial Electronics Society, vol. 4, pp. 176-188, 2023, doi: 10.1109/OJIES.2023.3278753.

[16] O. Lopez-Santos, D. Zambrano-Prada, L. Martinez-Salamero, A. E. Aroudi and L. Vazquez-Seisdedos, "Unidirectional DC-DC Converters for Ultrafast Charging of Electric Vehicles," 2023 IEEE International Conference on Electrical Systems for Aircraft, Railway, Ship Propulsion and Road Vehicles & International Transportation Electrification Conference (ESARS-ITEC), Venice, Italy, 2023, pp. 1-6, doi: 10.1109/ESARS-ITEC57127.2023.10114830.

[17] C. Yu et al., "High Efficiency Bidirectional Dual Active Bridge (DAB) Converter Adopting Boost-Up Function for Increasing Output Power," in IEEE Transactions on Power Electronics, vol. 37, no. 12, pp. 14678-14691, Dec. 2022, doi: 10.1109/TPEL.2022.3192048.

[18] Muqeet, H.A.; Liaqat, R.; Jamil, M.; Khan, A.A. A State-of-the-Art Review of Smart Energy Systems and Their Management in a Smart Grid Environment. *Energies* **2023**, *16*, 472. https://doi.org/10.3390/en16010472

[19] A. Raza et al., "Optimal Power Flow and Unified Control Strategy for Multi-Terminal HVDC Systems," in IEEE Access, vol. 7, pp. 92642-92650, 2019, doi: 10.1109/ACCESS.2019.2925049.

[20] M. M. Haque, P. Wolfs, S. Alahakoon, B. C. P. Sturmberg, M. Nadarajah and F. Zare, "DAB Converter With Q Capability for BESS/EV Applications to Allow V2H/V2G Services," in IEEE Transactions on Industry Applications, vol. 58, no. 1, pp. 468-480, Jan.-Feb. 2022, doi: 10.1109/TIA.2021.3123139.

[21] K.Y. Yap, C. Sarimuthu, and J. Lim, "Virtual Inertia-Based Inverters for Mitigating Frequency Instability in Grid-Connected Renewable Energy System: A Review," in Applied Sciences vol. 9, 2019, doi: 10.3390/app9245300.

[22] P. Yang, T. Peng, H. Wang, H. Han, J. Yang and H. Wang, "A single-phase current-source bidirectional converter for V2G application," 2017 IEEE 3rd International Future Energy Electronics Conference and ECCE Asia (IFEEC 2017 - ECCE Asia), Kaohsiung, Taiwan, 2017, pp. 704-709, doi: 10.1109/IFEEC.2017.7992125.

[23] A. K. Verma, B. Singh and D. T. Shahani, "Grid to vehicle and vehicle to grid energy transfer using single-phase bidirectional AC-DC converter and bidirectional DC-DC converter," 2011 International Conference on Energy, Automation and Signal, Bhubaneswar, India, 2011, pp. 1-5, doi: 10.1109/ICEAS.2011.6147084.

[24] O. Hegazy, J.V. Mierlo, P. Lataire, "Control and analysis of an integrated bidirectional dc/ac and dc/dc converters for plug-in hybrid electric vehicle applications," in J. Power Electron., vol. 11 no. 4, pp. 408-417, 2011, doi: 10.6113/JPE.2011.11.4.408

[25] C. Wei, J. Shao, B. Agrawal, D. Zhu and H. Xie, "New Surface Mount SiC MOSFETs Enable High Efficiency High Power Density Bi-directional On-Board Charger with Flexible DC-link Voltage," 2019 IEEE Applied Power Electronics Conference and Exposition (APEC), Anaheim, CA, USA, 2019, pp. 1904-1909, doi: 10.1109/APEC.2019.8721866.

[26] Texas Instruments, “GaN-Based, 6.6-kW, Bidirectional, Onboard Charger,” [Online]. Available: https://www.ti.com/tool/PMP22650.

[27] A. Pal and K. Basu, "A bidirectional snubber less soft-switched high frequency link DC/AC converter," 2016 7th India International Conference on Power Electronics (IICPE), Patiala, India, 2016, pp. 1-8, doi: 10.1109/IICPE.2016.8079423.